Carbon mineralization in Laptev and East Siberian Sea shelf and slope sediment

Volker Brüchert[1,3], Lisa Bröder[2,3], Joanna E. Sawicka[1,3], Tommaso Tesi[2,3,5], Samantha P. Joye[6], Xiaole Sun[4,5], Igor P. Semiletov[7,8,9], Vladimir A. Samarkin[6]

[1] Department of Geological Sciences, Stockholm University, Stockholm, Sweden
[2] Department of Environmental Sciences and Analytical Chemistry, Stockholm University, Stockholm, Sweden
[3] Bolin Centre for Climate Research, Stockholm University, Stockholm, Sweden
[4] Baltic Sea Research Center, Stockholm University, Stockholm, Sweden
[5] Institute of Marine Sciences – National Research Council, Bologna, Italy
[6] Department of Marine Sciences, University of Georgia, Athens, U.S.A.
[7] International Arctic Research Center, University Alaska Fairbanks, Fairbanks, USA
[8] Pacific Oceanological Institute, Russian Academy of Sciences, Vladivostok, Russia
[9] Tomsk National Research Politechnical University, Tomsk, Russia

Abstract The Siberian Arctic Sea shelf and slope is a key region for the degradation of terrestrial organic material transported from the organic carbon-rich permafrost regions of Siberia. We report on sediment carbon mineralization rates based on O_2 microelectrode profiling, intact sediment core incubations, ^{35}S-sulfate tracer experiments, porewater dissolved inorganic carbon (DIC), $\delta^{13}C_{DIC}$, and iron, manganese, and ammonium concentrations from 20 shelf and slope stations. This data set provides a spatial overview of sediment carbon mineralization rates and pathways over large parts of the outer Laptev and East Siberian Arctic shelf and slope and allowed us to assess degradation rates and efficiency of carbon burial in these sediments. Rates of oxygen uptake and iron and manganese reduction were comparable to temperate shelf and slope environments, but bacterial sulfate reduction rates were comparatively low. In the topmost 20 to 50 cm of sediment, aerobic carbon mineralization dominated degradation and comprised on average 84% of the depth-integrated carbon mineralization. Oxygen uptake rates and ^{35}S-sulfate reduction rates integrated over the topmost 30 cm of sediment were higher in the eastern East Siberian Sea shelf compared to the Laptev Sea shelf. DIC/NH_4^+ ratios in porewaters and the stable carbon isotope composition of remineralized DIC indicated that the degraded organic matter on the

Siberian shelf and slope was a mixture of marine and terrestrial organic matter. Based on dual end member calculations, the terrestrial organic carbon contribution varied between 32% and 36%, with a higher contribution in the Laptev Sea than in the East Siberian Sea. Extrapolation of the measured degradation rates using isotope end member apportionment over the outer shelf of the Laptev and East Siberian Sea suggests that about 16 Tg C per year are respired in the outer shelf sea floor sediment. Of the organic matter buried below the oxygen penetration depth, between 0.6 and 1.3 Tg C per year are degraded by anaerobic processes, with a terrestrial organic carbon contribution ranging between 0.3 and 0.5 Tg per year.

Key words: Carbon mineralization, Arctic shelf and slope sediment, Laptev Sea, East Siberian Sea

1. Introduction

The biogeochemical fate of terrestrial organic carbon deposited on the Arctic shelf and slope is one of the most important open questions for the marine Arctic carbon cycle (e.g., Tesi et al., 2014; Macdonald et al., 2015; McGuire et al., 2009; Vonk et al, 2012). The total pan-Arctic terrestrial permafrost region has been estimated to contain about 1100 – 1500 Pg, of which 500 Pg are seasonally or perennially unfrozen and contribute to the present-day carbon cycle (Hugelius et al, 2014). Additional partial thawing, mobilization, and oxidation of the perennially frozen carbon reservoir can substantially affect the global atmospheric carbon dioxide pool over the next 100 years (Schuur et al. 2015; Koven et al., 2015). A key problem in this context is the considerable uncertainty regarding the mineralization of terrestrial organic matter exported by rivers and coastal erosion to the Siberian shelf and slope (Tesi et al., 2014; Karlsson et al. 2015; Semiletov et al., 2011; Salvado et al., 2016).

Terrestrial organic matter transported to the Siberian shelf is of variable size, age, and molecular composition, which results in a range of different carbon degradation rates of bulk carbon and individual molecular components. Size class analysis of the organic matter suggests that coarse organic material settles preferentially in near-shore environments, whereas finer organic fractions disperse offshore in repeated deposition-resuspension cycles gradually losing particular molecular components and overall reactivity (Wegner et al., 2013; Tesi et al., 2014, 2016). Substantial oxic degradation of organic matter may occur during near-bottom transport in resuspension-deposition cycles across the shelf (Bröder et al.,

2016a). Up to 90% of certain biomarker classes may decompose during transport, whereby most of the degradation may take place while the transported organic material resides in the sediment before being resuspended (Bröder et al., 2016a). However, without making approximations on transport direction, particle travel time and travel distance these studies cannot provide direct insights into the rates of carbon degradation and resultant CO_2 fluxes from sediment. By contrast, direct kinetic constraints provided by sediment carbon degradation rates can provide testable data for coupled hydrodynamic biogeochemical models that help assess the fate of land-exported terrestrial carbon pool on the Siberian shelf.

Relatively few studies have directly measured rates of carbon mineralization rates in Siberian shelf sediment (e.g., Boetius and Damm, 1998; Grebmeier et al., 2006; Karlsson et al., 2015, Savvichev et al., 2007). Boetius and Damm (1998) used high-resolution oxygen microelectrode data to determine the surface oxygen concentration gradients and oxygen penetration depths in a large number of sediment cores from the shelf and slope of the Laptev Sea. Based on corresponding sediment trap and export productivity data, they concluded that the annual marine organic carbon export in the Laptev Sea shelf and slope was sufficiently high to explain the observed oxygen uptake rates. Current understanding therefore holds that due to the long annual ice cover and low productivity on the eastern Siberian Arctic shelf and slope, only a small amount of marine organic carbon is exported and buried in Laptev and East Siberian Sea shelf sediment. The highly reactive fraction of fresh organic matter is thought to degrade in the surface sediment (Boetius and Damm, 1998). Consequently, anaerobic respiration in buried sediment has been thought to be negligible and to reflect the degradation of unreactive terrestrially derived carbon compounds. To our knowledge, with the exception of a recent study by Karlsson et al (2015) a more direct assessment of terrestrial carbon-derived mineralization rates in buried shelf and slope sediment has not been reported for the East Siberian Arctic Sea.

In this study, we present data from oxygen microelectrode profiling experiments, porewater data of dissolved inorganic carbon and its stable carbon isotope composition, and ^{35}S-sulfate reduction rate experiments along a shelf-slope transect near 125°E in the Laptev Sea. Samples were taken during the summer 2014 on the SWERUS-C3 expedition with the Swedish icebreaker Oden. We combined these data with porewater analyses of dissolved ammonium, sulfate, iron, and manganese to assess the major carbon degradation pathways and rates across the extensive outer Laptev and Siberian shelf and slope.

2. Materials and methods

2.1. Sample collection

Samples were collected at 20 stations from 40 to 3146 m water depth in the western Laptev and East Siberian Sea (Fig. 1 and Table 1). In this study we only report on sampling sites that showed no methane gas plumes, acoustic anomalies in the water column, or sediment blankings indicative of rising gas. In areas of active ebullition from the seafloor as seen by video imagery and acoustic gas blankings in the water column, the biogeochemistry of sea floor processes such as bacterial sulfate reduction, DIC concentration and its carbon isotope composition, and oxygen uptake are affected by methane oxidation. These methane cycling-related signals overprint the biogeochemistry imparted by carbon mineralization and are reported in a separate study.

Sediment stations had variable ice cover (Table 1). In the Laptev Sea, except for the deep-water slope stations between 3146 m and 2106m, all stations had open water. By contrast, ice cover exceeded 75% in the East Siberian Sea to the west and east of Bennett island (Station 40 to 63). Sediments with well-preserved sediment surfaces were collected with a Multicorer (Oktopus GmbH, Kiel, Germany) that simultaneously takes 8 sediment cores over an area of about 0.36 m^2 with acrylic tubes (9.5 cm diameter, 60 cm length) to 40 cm depth preserving clear water on top of the sediment. At stations 6, 23, and 24, an underwater video system (Group B Distribution Inc., Jensen Beach, U.S.A.) was mounted on the multicore frame to record the deployment and recovery, and to document the sea floor habitat. For the investigations all cores were taken from the same cast. Two of the cores were used to determine ^{35}S-sulfate reduction rates and porosity. In addition, one core with predrilled 3.8 mm holes sealed with electric tape was used to extract porewaters with rhizons (Rhizosphere Research Products BV, Wageningen, Netherlands). A fourth core was used for microelectrode measurements of dissolved oxygen concentration profiling, and finally, four other cores were used for whole-core incubations to determine benthic fluxes of dissolved oxygen, dissolved inorganic carbon, and nutrients. The cores were capped with rubber stoppers until further subsampling usually within 30 minutes. For sulfate reduction rates, the cores were subsampled with 40 or 50 cm long acrylic tubes (26 mm inner diameter) prepared with silicon-sealed holes, drilled at distances of 1 cm. For whole-core incubations, the cores were sub-sampled with 25 cm-long, 60 mm-wide tubes (56 mm id) to 12 cm depth. Likewise,

a 60 mm diameter tube (56 mm id) was collected for microelectrode measurements preserving about 3 cm of the overlying bottom water. For intact whole-core incubations, temperature-controlled aquaria were filled with bottom water that was collected from a CTD rosette from the same station by collecting water from four ten-liter rosette bottles usually ~5 meters above the sea floor. All sediment cores were closed with a stopper retaining the water on top of the sediment and stored at 1.5°C in an incubator until further processing.

2.2. Microelectrode oxygen profiles

High-resolution O_2-profiles across the water-sediment interface were obtained to determine oxygen penetration depths and diffusive oxygen uptake (Rasmussen and Jørgensen, 1992; Glud, 2008) (Table 2). The 60 mm tubes were placed in an aquarium filled with bottom water from the same station, overflowing the sediment core. The water temperature was kept to ~1°C by a cooling unit (Julabo GmbH, Seelbach, Germany). In exceptional cases when there was not sufficient bottom water available to fill the aquarium, bottom water was used from a pump system. A stable diffusive boundary layer above the sediment was created by passing air from an aquarium pump over the water surface with a Pasteur pipette creating a slow rotational motion of water inside the core. At each station six to eight O_2 microprofiles were measured using Clark-type oxygen microelectrodes (OX-50, Unisense, Århus Denmark) mounted on a motor-driven micromanipulator (MM33, Unisense, Århus Denmark). O_2 sensors were calibrated with fully oxygenated bottom water from the same station at ~1°C for saturation and for anoxic conditions by dissolving Na_2SO_3 in the same water. The first profile in each core was measured with a resolution of 1000µm as a quick scan to locate the sediment surface and to adjust the measuring range. Then the vertical resolution was increased to 100-500µm and additional five to seven profiles were measured at different points on the surface, approximately one cm apart from each other.

2.3. Whole-core sediment incubations

Four intact cores with clear overlying water were subsampled in the laboratory in acrylic tubes (i.d. 56 mm, height 25 cm) retaining about 10 cm of the overlying water. The sediment and water height in the tubes were approximately 10 cm. The cores were incubated in a 40-liter incubation tank filled with bottom water from the same station. Before the

incubation the overlying water in the cores was equilibrated with bottom water in the tank. The overlying water in the cores was stirred by small magnetic bars mounted in the core liners and driven by an external magnet at 60 rpm. The cores were pre-incubated uncapped for 6 hours and subsequently capped and incubated for a period of 6 to 24 hours depending on the initial oxygen concentration in the bottom water. 2D oxygen sensor spots (Firesting oxygen optode, PyroScience GmbH, Aachen, Germany) with a sensing surface of a diameter of 5 mm were attached to the inner wall of two incubation cores. The sensor spots were calibrated against O_2-saturated bottom water and oxygen-free water following the manufacturer's guidelines accounting for temperature and salinity of the incubation water. Measurements were performed with a fiberoptic cable connected to the spot adapter fixed at the outer core liner wall at the spot position. The O_2 concentration was continuously logged during incubations. Sediment total oxygen uptake (TOU) rates were computed by linear regression of the O_2 concentration over time. 5 ml of overlying water were removed over the course of the incubation used for nutrient and dissolved CO_2 analysis as described below. Linear regression best fits were used to determine the exchange fluxes of dissolved CO_2.

2.4. Extracted porewater analysis

Porewater samples for concentration measurements of total dissolved inorganic carbon (DIC), sulfate, and ammonium were obtained using the methods described in Seeberg-Elverfeldt et al. (2005). Rhizons were treated for 2 hours in 10% HCl solution, followed by two rinses with deionized water for 2 hours and final storage in deionized water. The rhizons were connected to 10 mL disposable plastic syringes with inert pistons (VWR, Stockholm, Sweden) via polyethylene 3-way luer-type stopcocks (Cole-Parmer, U.S.A.) and inserted in 1-cm intervals through tight-fitting, pre-drilled holes in the liner of the sediment cores. The first mL of pore water was discarded from the syringe. No more than 5 ml were collected from each core to prevent cross-contamination of adjacent porewater due to the suction effect (Seeberg-Elverfeldt et al., 2005). The collected porewater was divided into four different aliquots for later chemical analysis. For dissolved sulfate analysis, 1 ml of porewater was preserved with 200 µl of 5% zinc acetate solution and frozen. For ICP-AES analysis of dissolved metals and major cations, 1 ml of porewater was preserved with 100 µl of 10% Suprapur HNO_3 and stored cold. For analysis of dissolved ammonium, 2 ml of porewater were frozen untreated. For analysis of dissolved inorganic carbon, 2 ml of porewater were preserved with 100 µl 10%

$HgCl_2$ and stored cold in brown glass vials without headspace. Ammonium was determined on a QUAATRO 4-channel flow injection analyzer (Seal Analytical) on board. All other porewater analyses were performed at the Department of Geological Sciences, Stockholm University. Samples that were analyzed in the home laboratory remained cold or frozen on board until arrival of the icebreaker Oden in Sweden. Sulfate concentration was measured on diluted aliquots on a Dionex System IC 20 ion chromatograph. DIC concentrations were determined by flow injection analysis (Hall and Aller, 1992). Dissolved iron and manganese were determined on diluted aliquots by ICP-AES (Varian Vista AX). For carbon isotope analysis of dissolved inorganic carbon, 1 ml of porewater was filled into 12 ml exetainers to which 1 ml of concentrated phosphoric acid was added. The carbon isotope composition of the formed CO_2 was analyzed on a GasbenchII-MAT 253 isotope ratio mass spectrometer coupled to a GC-PAL autosampler. Results are reported in the conventional delta notation relative to PDB. Precision of isotope analysis is 0.1‰.

For the calculation of porewater concentration ratios of DIC and NH_4^+, the effects of different diffusion coefficients and ammonium adsorption were accounted for. We have no direct measurements of adsorption coefficients for these sediments. Instead, we used an ammonium adsorption coefficient of 1.3 established for comparable, terrestrially dominated silty clays in the East China Sea for which similar porosities and organic carbon concentrations were reported (Mackin and Aller, 1984). The diffusion coefficient of HCO_3^- is about 45% smaller than the diffusion coefficient of NH_4^+ (Li and Gregory, 1974). The two effects required an upward correction of the ammonium concentration by 40% to facilitate direct comparison in DIC/NH_4^+ ratios. Diffusion- and adsorption-adjusted DIC/NH_4^+ ratios were also corrected for the bottom water DIC and NH_4^+ concentrations (Table 1). Only concentrations below 4 cm depth were used for comparison to avoid effects of oxidation on NH_4^+ concentrations.

2.5. Reaction transport modelling

Reaction rates and fluxes were estimated from the concentration profiles of dissolved oxygen, manganese, iron, and dissolved inorganic carbon according to the general reaction-transport equation at steady state accounting for diffusion and advection exemplified here for dissolved oxygen according to

$$\frac{d}{dz} = \left(\varphi(D_s + D_b)\frac{dO_2}{dz}\right) + \varphi\alpha\left(O_{2,\ z=0} - O_{2,\ z}\right) + \sum R = 0$$

(1)

At steady state, the rate of the concentration change reflects the balance between the consumption due to respiration and oxidation of reduced inorganic compounds (R) against diffusion and advection due to bioirrigation into sediment (Glud, 2008). D_s ($cm^2\ s^{-1}$) is the sediment diffusion coefficient and was calculated for the experimental temperature and salinity according to Boudreau (1997). The sediment diffusion coefficient D_s was recalculated from the molecular diffusion coefficient D_o according to $D_s = D_o / \theta^2$, where $\theta^2 = 1 - \ln(\varphi^2)$, where φ is porosity and θ is tortuosity (Boudreau, 1997). D_b ($cm^2\ s^{-1}$) is the bioturbation coefficient and α is the irrigation coefficient ($cm\ s^{-1}$). D_b and α were estimated by stepwise optimization by fitting a concentration profile to the measured data using the least square fitting procedure of the program Profile (Berg et al., 1998) testing various coefficients until the statistically best fit was obtained. Boundary conditions and the coefficients D_b and α for the best fits are shown in the supplemental material Table 1.

2.6. ^{35}S-Sulfate reduction rates

For the incubations, the whole-core incubation method by Jørgensen (1978) was used. $^{35}SO_4^{2-}$ tracer solution was diluted in a 6 ‰ NaCl solution containing 0.5 mM SO_4^{2-} and 2.5 µl of the tracer solution (200kBq) was injected through the pre-drilled holes. The cores were then capped and sealed in plastic wrap foil and incubated for 8 hours at the respective bottom water temperatures. After this time, the incubations were stopped by sectioning the core in 1-cm intervals to 5 cm depth and in two centimeter intervals below this depth to the bottom of the core. Sediment sections were transferred into 50 ml plastic centrifuge tubes containing 20 ml zinc acetate (20% v/v), mixed to a slurry on a vortex stirrer and frozen. The total amount of ^{35}S-labeled reduced inorganic sulfur (TRIS) was determined using the single-step cold chromium distillation method by Kallmeyer et al. (2004). TRIS and supernatant sulfate were counted on a TriCarb 2095 Perkin Elmer scintillation counter. The sulfate reduction rate was calculated using the following equation (Jørgensen, 1978):

$$^{35}SRR = \left(TRI^{35}S \times 1.045 \Big/ (^{35}SO_4^{2-} + TRI^{35}S) \right) \times [SO_4^{2-}]/\rho T \qquad (2)$$

where $[SO_4^{2-}]$ is the pore water sulfate concentration corrected for porosity ρ, $TRI^{35}S$ and $^{35}SO_4^{2-}$ are the measured counts (cpm) of sulfate and total reduced inorganic sulfur species, respectively, 1.045 is a correction factor accounting for the kinetic isotope effect of ^{35}S

relative to ^{32}S, and T is the incubation time. The sulfate reduction rate is reported as nmol cm^{-3} day^{-1}. ^{35}SRR were measured in two parallel cores for all depth intervals. The incubation experiments were conducted between July 15 and August 20, but for logistical reasons (transport to Stockholm) the distillation of the samples was conducted between December 10, 2014 and April 2, 2015 so that between 1.7 and 2.7 half-lives of ^{35}S (87.4 days) had passed before all samples were processed. The resulting detection limit of the rate measurements accounting for distillation blanks and radioactive decay of ^{35}S between experiment and laboratory workup was 0.01 nmol cm^{-3} day^{-1}.

2.7. Carbon equivalent apportionment of terminal electron-accepting processes

The modelled oxygen, iron, manganese, and DIC reaction rates were integrated over 30 cm sediment depth to permit comparison between different stations. The integrated terminal electron accepting processes (TEAP) were recalculated into carbon equivalents for the electron acceptors oxygen, iron, manganese, and sulfate using an idealized $(CH_2O)_x$ stoichiometry for organic matter (Vandieken et al., 2006; Nickel et al., 2008). The calculated rates were then used to calculate the contribution of the different aerobic and anaerobic electron acceptors to total carbon mineralization for 5 stations in the Laptev and East Siberian Sea (Table 3).

2.8 Marine versus terrestrial endmember partitioning of carbon degradation rates

In order to determine the proportion of mineralized terrestrial and marine organic matter in the sediment directly, we used the DIC concentration and the carbon isotope composition of DIC to determine the contribution of remineralized organic matter to porewater DIC using a simple isotope mass balance model. Porewater DIC is assumed to be derived from bottom-water DIC and remineralization of organic matter during burial. We used a Keeling-type plot of 1/DIC against the corresponding stable carbon isotope composition of DIC to determine the isotope composition of the remineralized endmember by linear regression. The method assumes that diffusion is slow compared to burial and mineralization and that isotope fractionation during the oxidation of organic matter is negligible. Removal or addition of DIC by diagenetic processes such as $CaCO_3$ precipitation or dissolution were minor. This is supported by the observation that the porewater

concentrations of Ca^{2+} and Mg^{2+} at these shelf and slope stations did not change significantly with depth (Brüchert and Sun, unpubl. data). The relative contribution of the terrestrial and marine organic carbon was calculated with a linear two-endmember isotope model:

$$\delta^{13}C_{DIC,\ remineralized} = f_{terr} * \delta^{13}C_{terr\ OC} + f_{mar} * \delta^{13}C_{marine\ OC} \quad (4)$$

where f_{terr} and f_{mar} are the respective mass fractions of terrestrial and marine-derived organic carbon and $\delta^{13}C_{terr\ OC}$ and $\delta^{13}C_{marine\ OC}$ reflect the isotope composition of these endmembers. For the Laptev Sea shelf, a fraction of the surface water DIC used for marine production is derived from terrestrial DOC and POC remineralized in shelf waters and transported from land (Humborg et al., 2017; Tesi et al., 2017; Alling et al., 2012). $\delta^{13}C$ values of offshore sediment in the Laptev Sea sediment are as heavy as -22.3 ‰ (Salvado et al., 2016). Tesi et al (2017) report $\delta^{13}C$ of POC of -24.7 ‰ for outer Laptev Sea POC near the ice edge containing abundant dinoflagellates and only trace indicators of terrestrial organic carbon. Based on these data we use an isotope endmember composition of -23.0 ‰ for marine organic matter in the Laptev Sea. We are aware that there may be regional variations in this endmember composition. An isotope composition of -28 ‰ was used for the terrestrial organic carbon contribution in the Laptev Sea (Vonk et al., 2012). For the East Siberian Sea east of 140°E, the heaviest calculated isotope composition of remineralized porewater DIC was -19 ‰ and is used here as the marine endmember (Station 53). The same carbon isotope composition of -28 ‰ as for the Laptev Sea was used as the terrestrial end member. In order to derive specific degradation rates of the marine and terrestrial carbon fractions, the endmember mixing-based assessment of the marine and terrestrial organic carbon contributions to DIC were combined with the mineralization rates derived for the different electron acceptors.

3. Results

3.1. Physical and chemical bottom water conditions

Table 1 summarizes the general site characteristics of the investigated sediment stations. Bottom water salinity varied between 34.9 ‰ in the outer Laptev Sea at 3146 m depth (Station 1) to 29.1 ‰ in the East Siberian Sea at 40 m (Station 45). The lower salinity in the East Siberian Sea can be attributed to longshore transport of freshwater eastward from the Lena River. Bottom water temperatures varied between -1.8°C at Station 27 and 0°C at

Station 37, but there was no regional trend in the data. Cored sediment consisted of silty clays to clayey silts. Slope sediment had a distinctly brown color throughout the cored interval, whereas shelf sediment only had a 1 to 4 cm-thick brown interval, below which the sediment color changed to grey. In the eastern part of the East Siberian Sea, the sediment was mottled black below 10 cm depth. Iron-manganese concretions were found between 2 cm and 10 cm depth at stations 24, 42, and 43, but were also observed at other stations on the shelf that were not part of this study. Benthic macrofauna, when present, consisted mainly of brittle stars, isopods, few polychaetes, and rare bivalves. All bottom waters were well-oxygenated with concentrations higher than 190 µmol/l, but the shelf bottom-waters in the East Siberian Sea had generally lower concentrations than in the Laptev Sea and bottom waters on the continental slope had lower oxygen concentrations than on the shelf. Concentrations of bottom-water ammonium ranged between 0.2 µmol/L and 1.8 µmol/L. Generally, the slope stations and the shelf stations nearest to the Lena delta had the highest ammonium concentrations, whereas the other shelf stations showed no clear regional trend other than proximity to the Lena delta. Bottom water dissolved inorganic carbon concentrations varied between 2086 µM (Station 53) and 2598 µM (Station 27), and the stable carbon isotope composition of DIC in the waters overlying the cores were between -0.5 ‰ and -6.5 ‰ vs. VPDB.

3.2. Dissolved oxygen, manganese, and iron

We show representative profiles of oxygen concentrations in Figure 2 for the Laptev Sea slope station 1, the Laptev Sea shelf stations 23, 30, 45, and the East Siberian Shelf Sea 53 and 63. Oxygen penetration depths varied between 3 mm at Station 58 and more than 60 mm in all slope sediments (Table 2). For the Laptev Sea slope stations 1, 2, 3, and 4, the maximum depth of oxygen penetration could not be determined, because at penetration greater than 60 mm the conical sensor needle opened a hole in the sediment through which oxygen-containing bottom water could potentially have entered the sediment at depth thereby artificially extending the oxygen penetration depth. In the slope-to-shelf transects the oxygen penetration depth decreased from >60 mm off-shore to 10 mm at the most inshore station in the Laptev Sea and the East Siberian Sea. At the two easternmost shelf stations 58 and 63, we measured the lowest oxygen penetrations depths, 3 mm and 4 mm, respectively. Evidence for bioturbation and bioirrigation based on multiple microelectrode profile measurements per

core was rare. Only at Station 48 a clear increase in oxygen concentrations below the sediment surface was observed, indicative of active bioirrigating macrofauna. However, even at this station, based on investigations in parallel multicore casts, fauna was not abundant (A. Gukov, pers. comm.). At all other stations, oxygen concentrations decreased exponentially with depth. Fitting of the oxygen concentration profiles to the steady advection-diffusion-transport model (Eq. 1) yielded fluxes that varied between 0.81 and 11.49 mmol m^{-2} d^{-1} (Table 2). These calculated O_2 fluxes compared well with total oxygen uptake rates calculated from whole-core incubations using 2D optode sensor spots (Table 2). The good fit between the two methods also supports the notion that bioirrigation and bioturbation effects from meiofauna and macrofauna were minor.

In the slope sediment at Station 1, concentrations of dissolved manganese and iron were low throughout the cored depth interval and below 0.2 and 0.5 µM, respectively. The exception was a small increase for both elements between 4 and 8 cm depth and 14 and 20 cm depth to concentrations of less than 3 µM, possibly due to slightly more degradable organic material in these depth intervals (Fig. 2). A similar concentration profile was found for the other slope station 4 (data not shown), but here concentrations were below 2 µM throughout for both dissolved iron and manganese and only slightly higher in the topmost cm. On the shelf, in the Laptev Sea (Station 23 and 30), concentrations of dissolved manganese and iron were below 0.3 µM and 1.5 µM, respectively, in the top 2 cm and 3 cm at Station 23, before increasing to maximum concentrations of 69 and 134 µM. At both stations, metal concentrations decreased again below the concentration maximum indicating that deeper buried sediment was not a source of the metals and that the dominant source of iron and manganese was reduction in the topmost 5 cm of sediment. There was a general trend of increasing manganese concentrations from west to the east. At Station 30 in the Laptev Sea, the concentration of dissolved manganese was less than 0.3 µM in the topmost cm, but increased steeply before increasing to maximum concentrations of 189 µM at 9 cm depth. Similarly, dissolved iron concentrations were below 1 µM to 4 cm depth and then increased to 144 µM. Again, below the maximum, both iron and manganese porewater concentrations decreased with increasing sediment depth. Even higher iron and manganese concentrations were found in the East Siberian Sea (Stations 45, 53, 63), where dissolved manganese already increased from the bottom water to concentrations of 20 µM in the topmost centimeter of sediment, and iron increased to above 1 µM below 2 cm depth. The steepest manganese concentration gradient was found at Station 63 in the easternmost East Siberian Sea, where

concentrations were 501 µM in the first cm of sediment with a concentration maximum of 548 µM at 2.5 cm depth and decreasing below this depth to 115 µM at 30 cm depth. Station 63 differed with respect to dissolved iron concentrations from the other stations, because here dissolved iron showed two small peaks at 3.5 cm and 7 cm, and concentration increased substantially only below 17 cm depth to concentrations of 189 µM.

3.3. ^{35}S-sulfate reduction rates and porewater sulfate

Sulfate concentrations showed minor depth gradients at all sampling sites (Fig. 3) and decreased from starting concentrations between 23.9 mM and 28.1 mM by 0.4 mM to 2.5 mM from the top to the bottom of the cores. At all stations, turnover of ^{35}S-tracer was recorded from the topmost sediment interval to the bottom of the core indicating active bacterial sulfate reduction (Fig. 3). Depth-integrated rates over the recovered core lengths varied between 0.03 and 1.41 mmol m^{-2} d^{-1} (Table 2). The integrated rates were lowest at Station 1 at 3146 m in the Laptev Sea and highest at the Station 63 in the easternmost East Siberian Sea. Across the shelf (Stations 6 to 24), depth-integrated rates increased from the west to the east. Example depth profiles of depth-specific sulfate reduction rates are shown in Fig. 3 for the same six stations as previously. At Station 1, these rates ranged from 0.03 to 0.38 nmol cm^{-3} d^{-1}. At this station, the variability between replicate cores was large, which is attributed to the fact that many rates were near the detection limit in our handling procedure. Overall, sulfate reduction was higher in the top 10 cm of sediment, but showed no pronounced change with depth at this station. This suggests that the reactivity of the organic material did not change substantially over the cored depth interval. The second slope station, Station 4, showed a similar rate-depth profile than Station 1. Depth profiles for the mid-outer shelf stations 23 to 63 all showed broad sub-surface maxima between 2.5 and 17.5 cm, but the depths of the rate maxima differed between the different stations (Fig. 3). Peak rates varied between 0.6 nmol cm^{-3} d^{-1} at Station 30 and 39 nmol cm^{-3} d^{-1} at Station 63. The second highest rate, 7.6 nmol cm^{-3} d^{-1}, was found at the station nearest to the Lena delta, Station 23. At all stations, sulfate reduction rates decreased from the maxima to rates below 1 nmol cm^{-3} d^{-1} or to below the detection limit at the bottom of the cores. A particularly sharp decrease in the sulfate reduction rate was observed between 8 and 9 cm at Station 63, where rates dropped from 8.5 to 0.1 nmol cm^{-3} day^{-1} over 1 cm depth. Since sulfate was abundant throughout the cored intervals, this order-of-magnitude decrease indicates substantial changes in the reactivity of buried organic matter.

412 Although no abrupt change in grain size or organic carbon was observed in this core, it is
413 likely that a historical change in organic sedimentation took place during deposition across
414 this time interval.

415

416 **3.4. Porewater dissolved inorganic carbon (DIC), ammonium (NH_4^+), and $\delta^{13}C_{DIC}$**

417 Porewater concentrations of dissolved inorganic carbon (DIC) and ammonium (NH_4^+)
418 increased with depth at all stations (Fig. 4). The increase of DIC was between 0.6 mM
419 (Station 23) and 2.3 mM (Station 45) over the cored sediment depths and ammonium
420 concentrations increased between 16.8 µM (Station 1) and 549 µM (Station 50). The
421 steepness of the depth gradients was consistent with the rates of oxygen uptake and bacterial
422 sulfate reduction for the different stations. The porewater pattern at Station 63 was an
423 exception, because this station had the highest oxygen uptake and the highest sulfate
424 reduction rates of all stations, but showed only a modest increase in DIC and NH_4^+
425 concentrations by 1.5 mM and 57 µM, respectively, over the cored sediment depth. The low
426 DIC concentrations are consistent with the very low rates of sulfate reduction below 10 cm
427 depth. Since these deeper layers have not produced large amounts of DIC and NH_4^+, only the
428 surface 10 cm contribute significantly to total carbon mineralization and ammonium
429 production.

430 For the anoxic parts of the sediment, DIC/NH_4^+ ratios varied between 8.4 for Station 24 and
431 40 respectively for Stations 1 in the Laptev Sea, and between 7.2 and 18.8 in the East Siberian
432 Sea, with an overall mean DIC/NH_4 ratio of 9.8 for all stations excluding the continental slope
433 stations (Fig. 5a). The $\delta^{13}C$ values of DIC consistently decreased with sediment depth
434 indicating the addition of ^{13}C-depleted remineralized carbon to DIC. The greatest downcore
435 depletion in ^{13}C was observed at stations 45, 48, and 50, where $\delta^{13}C$ of DIC decreased from -
436 2.0 ‰ near the sediment surface to -13.9, -16.4, and -18.6 ‰ at the bottom of the cores (Fig.
437 4).

438 Fig. 5b shows Keeling plots for the six stations presented before and Table 4 lists the derived
439 carbon isotope compositions of remineralized organic matter for all stations. The range of
440 $\delta^{13}C$ of remineralized DIC varied between -18.8 ‰ ± 1.1 ‰ (Station 53) and -35.8‰ ± 3.0 ‰
441 in the lower part of Station 1. At this station, the data for the topmost 20 cm yielded an
442 isotope composition of -22.7 ‰ for remineralized DIC. This isotopic composition reflects the

443 bulk organic matter composition of sedimentary organic carbon at this station, which is -22.3
444 ‰ (Salvado et al (2016). The more depleted values below 20 cm depth suggest that an
445 isotopically distinct fraction of organic matter fuels carbon degradation in the buried
446 sediments. Salvado et al (2016) report terrestrial-derived lignin from sediment at this station
447 pointing to the presence of terrestrial organic matter. Terrestrially derived n-alkanes can have
448 such low $\delta^{13}C$ values (Pagani et al., 2006). Slow degradation of terrestrially derived lipids in
449 these sediments suggests a contribution of terrestrial organic matter to carbon mineralization
450 far offshore, in line with the very high DIC/NH_4^+ ratio of the porewaters at the slope stations.
451 The contribution of degradable terrestrial organic matter to DIC in lower slope sediments is
452 also supported by the observation of terrestrially derived biomarkers in porewater DOC of
453 central Arctic Ocean sediment analyzed by FT-ICRMS (Rossel et al., 2016) and deep-water
454 sediment trap data in the central Arctic Ocean (Fahl and Nöthig, 2007), but requires further
455 investigation.

456 The calculated mass fractions of the marine and terrestrial endmembers are listed in Table 4.
457 In the Laptev Sea on average 47 % of the remineralized DIC is derived from terrestrial
458 organic carbon. This proportion decreases to an average value of 32% in the East Siberian
459 Sea, in line with a greater marine production in this area due to the inflow of Pacific water
460 (Semiletov et al., 2005, Dudarev et al., 2006; Naidu et al., 2000).

461

462 **3.5. Benthic exchange and modelled oxygen, iron, and manganese reduction rates**

463 Benthic exchange fluxes from whole-core incubations and modelled DIC fluxes are
464 shown in Table 2. A good agreement was found between 2D oxygen optode flux
465 measurements and the modelled O_2 concentration fluxes, whereas the modelled DIC fluxes
466 were generally lower than the whole-core incubation fluxes. We attribute this discrepancy to
467 an underestimation of the DIC gradient at the sediment-water interface. A representative
468 result of the reaction transport modelling for dissolved oxygen, iron, and manganese is shown
469 for Station 23 in Fig. 6. Optimal fits of the concentration profiles required a bioirrigation
470 coefficient of 1 x 10^{-4} cm^2 sec^{-1} in the topmost 2 cm of sediment at Stations 23 and 53. For the
471 other stations, optimal fits required no sediment mixing by bioturbation or advective
472 porewater transport by bioirrigation. This is consistent with the low numbers of bioturbating
473 macrofauna in the outer shelf sediment. O_2 consumption rates exceeded sulfate and net
474 reduction rates of iron and manganese by a factor of 100 (Fig. 6). On the shelf, most of the

carbon oxidation therefore takes place in the topmost 5 mm. The reaction rate depth profiles for iron and manganese indicate that manganese reduction dominates in the topmost 2 cm of sediment followed by co-existing iron and sulfate reduction below (Fig.6). Bacterial sulfate reduction was already detected at a depth where the sediment was still brown indicating abundant iron and manganese hydroxides. Coexistence of net iron reduction and sulfate reduction at the same depths make it difficult to quantify how much of the iron reduction is coupled to heterotrophic carbon oxidation and to the re-oxidation of sulfide produced from bacterial sulfate reduction. Qualitatively, the presence of dissolved iron throughout the measured porewater profile implies that iron reduction exceeded concomitant sulfate reduction, iron sulfide precipitation, and reoxidation reactions, which supports the assessment of net heterotrophic iron reduction. However, previous investigations of the importance of iron and manganese reduction in Arctic shelf sediments have emphasized the importance of coupled redox processes between iron and manganese and sulfide (Vandieken et al., 2006). It is also important to note that iron and manganese oxyhydroxides can sorb Mn^{2+} and Fe^{2+} (Canfield et al. 1993). The concentrations of dissolved Fe^{2+} and Mn^{2+} may therefore underestimate the actual concentrations of the reduced forms in these sediments. Assuming no direct redox coupling between the terminal electron-accepting processes, manganese and iron reduction contributed maximally between 2.3 and 23.7% to the total anaerobic carbon mineralization and between 0.3 and 2.3% to the total carbon mineralization (Table 3). Even if these numbers overestimate the contribution of metals to carbon mineralization, the results indicate that bacterial sulfate reduction is by far the major anaerobic carbon mineralization pathway in these sediments. The prevalence of bacterial sulfate reduction in anaerobic carbon mineralization agrees with results of Vandieken et al. (2006) and Nickel et al. (2008) from the northern Barents Sea where ice-free stations supported higher rates of sulfate reduction than the more permanently ice-covered stations reflecting lower carbon export production.

The modelled negative iron production rates at the sediment surface indicate net iron oxidation by oxygen in the mixed upper sediment layer. This pattern was not observed for manganese, which is consistent with incomplete manganese oxidation at the sediment surface and loss of dissolved manganese to the bottom water. The efflux of manganese to the bottom water on the eastern Siberian shelf supports results by Macdonald and Gobeil (2012) that Arctic shelves can export dissolved manganese to the Arctic interior. Consistent with these observations there was a statistically significant positive correlation between the dissolved oxygen uptake and anaerobic carbon degradation rates by sulfate reduction (r^2 0.75, $P < 0.05$)

(Fig. 7). This reflects the coupling of oxygen uptake to the oxidation of reduced inorganic metabolites (FeS and H_2S) produced during sulfate reduction (e.g., Glud, 2008; Jørgensen and Kasten, 2006; Thamdrup, 2000; Berg et al., 2003). The slope of the regression line for all stations at which sulfate reduction rates were determined was 6.1±1.1. The percentage of the inverse of this slope, 16.4 %, reflects the average oxidation of reduced manganese, ammonium, dissolved iron, iron sulfides, and elemental sulfur by oxygen. This amount is slightly lower than the average 23% estimated for oxygenated coastal and continental shelf sediment (Canfield et al., 2005), but is consistent with the notion that a substantial amount of the buried organic matter in Siberian shelf sediment is oxidized anaerobically. The lower proportion of anaerobic respiration to aerobic respiration compared to other shelf environments likely reflects the greater proportion of highly reactive marine-derived organic material in the topmost millimeters of sediment.

4. Discussion

4.1. Marine versus terrestrial organic matter contribution

Terrestrial organic carbon sources to the Laptev and East Siberian shelf and slope are riverine discharge and coastal erosion of the ice core complex (Stein and Macdonald, 2004; Vonk et al., 2012; Rachold et al., 2004; Fahl and Nöthig, 2007; Semiletov, 1999). Marine organic carbon is derived from open-water production during the ice-free months, export of ice algae, and new production in polynyas (Sakshaug et al., 2004; Nitishinsky et al. 2007). Generally, marine productivity in the Laptev Sea is low and controlled by the nutrient concentrations derived from Atlantic water, but spring outflow from the Lena River provides an additional temporary land-derived nutrient source (Pivovarov et al., 1999; Sakshaug et al., 2004; Nitishinsky et al., 2007; Bourgeois et al., 2017) during late spring ice melt (Raymond et al., 2007). Terrestrial-derived nutrients can also affect marine productivity either directly by new production, or indirectly, due to plankton production from remineralized terrestrial dissolved organic carbon and particulate organic carbon (Alling et al., 2012; Tesi et al., 2017). In the eastern East Siberian and Chukchi Sea, the inflow of nutrient-rich Pacific water supports higher marine primary productivity (e.g., Grebmeier et al., 2006). Ice-rafted transport and bottom boundary layer transport are the two most important modes of particle transport (Wegner et al., 2005; Bauch et al., 2009). Since all sediments sampled in this study were fine-grained siltey clays and clayey silts, coarse-grained woody, ice-rafted material plays only a

minor role for deposition of organic matter on the outer shelf and slope sediment. The transport direction of inner shelf sediments has been suggested to follow the predominant atmospheric regime, which is thought to be linked to the Arctic Oscillation (AO) (Dimitrenko et al., 2008; Guay et al., 2001; Weingartner et al., 1999). During positive AO southwesterly winds lead to generally eastward transport and repeated inshore transport in the benthic boundary layer, whereas negative AO favors southerly winds and a predominantly northward transport (Guay et al., 2001; Dmitrenko et al., 2008). Offshore transport of dissolved and particulate organic matter from the Lean delta to the north can occur with the Transpolar Drift, but terrestrial organic material is also transported eastward and obliquely offshore with the Siberian coastal current receiving additional organic material from the Indigirka and Kolyma rivers (Guo et al., 2007; Dudarev et al., 2006). East of 140ºE, the influence of Pacific-derived nutrient-rich water supporting marine production is stronger the further east and offshore the sampling stations are located (Semiletov et al., 2005) (Fig. 1).

Carbon degradation rates in the sediment across the whole Siberian shelf and slope reflect this temporally and spatially diverse distribution of nutrient availability, ice cover, sediment deposition, and current flow regime (Rachold et al., 2004; Dudarev et al., 2006; Semiletov et al., 2005; Sakshaug et al., 2004; Dmitrenko et al., 2005). The proportion of degradable marine-derived organic material at the eastern Stations 50 to 63 on the East Siberian shelf is higher than at the western stations in the Laptev Sea, in line with higher nutrient availability due to the Pacific influence. Ice-free conditions and the opening of water due to northward migration of ice shortly before the sampling likely supported new algal primary production at the shelf stations closest to land leading to enhanced export and deposition on the seafloor. During the time of sampling, only Stations 6 to 27 were ice-free, while Stations 23 and 24 had the longest ice-free condition before sampling. By contrast, Stations 30 to 63 were covered by ice during sampling. New export of reactive organic material explains why O_2 uptake rates were the highest at stations 23 and 24 along the shelf to slope transect from station 1 to station 24 (Boetius and Damm, 1998). The same pattern as for the O_2 uptake rates is also observed for the sulfate reduction rates indicating that reactive organic matter is also buried below the oxygen penetration depth and mixed sediment layer into the sulfate-reducing zone. This indicates that a greater portion of reactive organic material is buried closer to the Lena delta.

Published organic carbon budgets for the Arctic shelves infer an average burial efficiency of about 1% of exported marine OC (Stein and Macdonald, 2004), while terrestrial

573 organic carbon, only accounting for about 10% of the organic carbon delivered to the Arctic
574 Ocean bottom, has been suggested to be preserved with about 90% efficiency (Macdonald et
575 al., 2015). Semiletov et al. (2016) compiled a large dataset indicating substantial aragonite
576 undersaturation of Arctic shelf bottom waters from the Laptev, the East Siberian, and the
577 Russian part of the Chukchi Sea and inferred widespread remineralization of terrestrial
578 organic matter in the bottom waters and sediments. The observation of strongest aragonite
579 undersaturation in the bottom waters supports a sediment-derived CO_2 source or a stagnant
580 bottom boundary layer (Semiletov et al., 2013). It is therefore possible that oxic carbon
581 mineralization in the topmost mm of sediment is a major CO_2 source for the overlying water.

582 Since ^{35}S-sulfate reduction rates comprise most of the anaerobic carbon mineralization
583 of sediment buried below the oxygen penetration depth, our assessment includes, in contrast
584 to earlier studies, an assessment of terrestrial organic matter mineralization beyond the short
585 time period of oxygen exposure in the topmost mm of sediment. Using sedimentation rates of
586 0.8 mm y^{-1} for the outer Laptev Sea (Strobl et al., 1988) and 1.4 mm y^{-1} for the outer East
587 Siberian Sea (Bröder et al., 2016b), the recovered sediments record a time interval of 250 to
588 700 years since burial. Using the mass fractions of terrestrial and marine-derived organic
589 carbon listed in Table 4, respective mineralization rates of the terrestrial and marine carbon
590 fractions were calculated from the product of the mass fractions and the depth-integrated
591 anaerobic carbon mineralization rates from Table 2. This approach is only applicable for
592 depth-integrated anaerobic carbon mineralization rates and is not possible without making
593 assumptions for oxic carbon mineralization. The depth of oxygen penetration varied only
594 between a few millimeters to little more than a centimeter on the shelf, whereas the
595 corresponding DIC concentration profiles, from which the marine and terrestrial proportions
596 were derived, are affected by diffusive exchange along the 30 cm-long concentration profile.
597 It is therefore not possible to assess the relative fractions of terrestrial and marine organic
598 matter mineralized for discrete depth intervals or the oxic zone. Nevertheless, our combined
599 radiotracer and DIC stable isotope approach suggests that both marine and terrestrial organic
600 matter are degraded in the buried anoxic sediment. This assessment is a significant
601 modification to earlier studies by Boetius and Damm (1998) and Bourgeois et al. (2017), who
602 have described organic matter mineralization in Siberian Arctic sediments largely as a
603 function of oxygen uptake.

604 Carbon mineralization rates measured along the transect near 130ºE (Stations 1 through
605 24) reflect the influence of gradual offshore transport of terrestrial organic material (Bröder et

606 al., 2016a) (Fig. 8A, B). Oxygen uptake rates reported by Boetius and Damm (1998)
607 measured in the early fall of 1993 ranged between 0.16 and 1.56 mmol m^{-2} d^{-1}. The data range
608 in our study (0.81 to 11.49 mmol m^{-2} d^{-1}) covers the same water depth range and indicates that
609 all rates measured in 2014 were significantly higher than the rates measured in 1993 by
610 Boetius and Damm (1998) (Student's t-Test <0.01, one-tailed distribution, heteroscedastic).
611 To some extent the different rates may reflect a seasonal effect, because Boetius and Damm's
612 data were acquired later in the year than our data. However, the increase may also point to
613 higher organic carbon mass accumulation rates compared to 20 years ago, consistent with a
614 decrease in the annual ice cover over the past 20 years in the Arctic (Arrigo and van Dijken,
615 2011; Stroeve et al., 2012; Walsh et al., 2017). Whether these rates reflect higher marine
616 and/or terrestrial accumulation cannot be answered satisfyingly with this data set.

617 Fig. 9A compares the oxygen uptake rate of the stations of this study with averaged
618 oxygen uptake rates from the literature for different shelf, slope, and abyssal plain
619 environments worldwide (Canfield et al., 2005). The data suggest that there is no significant
620 difference in the oxygen consumption rates between the Siberian shelf and slope and other
621 continental margin environments(Student's T-test >0.5, one-tailed distribution,
622 heteroscedastic). ^{35}S-sulfate reduction rates in these East Siberian slope sediments are also
623 comparable rates to those in other slope environments (Fig. 9B), but the sulfate reduction
624 rates on the shelf are lower by a factor up to 15. Another difference apparent from this
625 comparison is the similarity in sulfate reduction rates for the outer shelf and continental slope
626 sediments of the Siberian Arctic (Fig. 9B). This similarity suggests that the kinetics of
627 anaerobic carbon degradation in the shelf and slope sediments reflect similar reactivity of the
628 organic matter. This is surprising since accumulation rates on the continental slope are
629 probably significantly slower than on the outer shelf. 2) The absolute magnitude of the sulfate
630 reduction rates in shelf and slope sediment indicate significant rates of organic matter
631 mineralization long after burial consistent with the substantial DIC flux and the strongly ^{13}C-
632 depleted DIC carbon isotope composition. Overall, the data indicate that organic matter
633 reactivity substantially changes during burial in shelf sediment, but that the reactivity of
634 transported organic matter that is exported to deep water across the shelf does not decrease
635 significantly supporting further long-term slow mineralization rates in the slope environment.
636 Accumulation of the organic material on the slope may therefore be related to rapid
637 downslope transport of organic material or a rapid offshore transport, e.g., due to transport

638 with ice or as bottom nepheloid layers cascading from the shelf edge (Ivanov and Golovin,
639 2007).

640

641 **4.2. Assessment of carbon burial efficiency**

642 Reported ^{210}Pb-based sediment accumulation rates in outer Siberian shelf sediment
643 range between 0.05±0.02 g cm^{-2} y^{-1} in the Laptev Sea (Strobl et al., 1988) and 0.24±0.04 g
644 cm^{-2} y^{-1} in the East Siberian Sea (Bröder et al., 2016b). Given surface sediment organic
645 carbon concentrations for this area between 1% and 1.5%, the resulting organic carbon mass
646 accumulation rates vary between 1.1 mmol m^{-2} d^{-1} and 1.7 mmol m^{-2} d^{-1} for the Laptev Sea
647 (area near Station 23) and between 5.5 and 8.2 mmol m^{-2} d^{-1} in the East Siberian Sea (data for
648 Station 63). A comparison of the total oxygen uptake with the C_{org} mass accumulation rates
649 indicates that the ^{210}Pb-based C_{org} mass accumulation rates on the shelf are equal or
650 significantly lower than the oxygen uptake rates, with a discrepancy of up to a factor 10.
651 Since the derivation of the ^{210}Pb-based C_{org} mass accumulation rates is based on the same
652 depth range as our direct degradation rate measurements (30 cm of sediment, Vonk et al.,
653 2012), C_{org} mass accumulation rates and anaerobic degradation rate measurements cover the
654 same time window of sediment burial. Temporal variation in sediment accumulation therefore
655 cannot explain the discrepancy. The best explanation is that the ^{210}Pb-mass accumulation rates
656 underestimate the true C_{org} mass accumulation rate. Labile organic carbon is oxidized at the
657 sediment surface and not adequately accounted for in the C_{org} measurements, likely due to
658 coarse sediment sampling resolution. A better account of the true mass accumulation of
659 organic carbon is therefore the sum of the oxygen uptake converted to CO_2 equivalents plus
660 the ^{210}Pb-based C_{org} mass accumulation.

661 We estimated the total burial efficiency of organic carbon from the sum of the depth-
662 integrated aerobic and anaerobic degradation relative to the sum of the CO_2 equivalent from
663 O_2 uptake and the ^{210}Pb mass accumulation rate of organic carbon. The resulting burial
664 efficiency of the total organic carbon is on average 28 ± 10 % in the Laptev Sea and 52 ± 11
665 % for the East Siberian Sea. Based on the measured oxygen uptake rates this freshly deposited
666 organic material has substantially higher degradation rates within the top mm of sediment as
667 reflected by the steep O_2 gradients. It is likely that this labile fraction consists of both
668 terrestrial and marine organic matter, but the degradation kinetics of these two pools cannot
669 be assessed reliably.

670

671 **4.3. Regional estimates**

672 We present areal estimates of sediment carbon mineralization by extrapolating the
673 measured carbon mineralization rates over the outer Laptev Sea and East Siberian Sea shelf.
674 Such extrapolations of benthic carbon mineralization rates are notoriously difficult given
675 sediment heterogeneity and insufficient temporal data coverage of benthic carbon
676 mineralization rates. For this investigation, no near-shore or slope stations were included in
677 the assessment. The near-shore Siberian shelf environments are under much stronger
678 influence by coastal erosion and riverine discharge than the outer shelf stations and have
679 considerable longer open-water conditions than the outer shelf stations investigated here. In
680 addition, the sedimentation pattern in the near-shore environments is significantly more
681 diverse, which will affect sedimentation rates, grain size distribution, and carbon contents. For
682 this reason, we did not extend our extrapolations to the inner shelf environments. Some of
683 these inner shelf settings likely have much higher benthic carbon mineralization rates and
684 additional studies are required to constrain these better. Our coverage of the slope stations is
685 insufficient for meaningful spatial extrapolations.

686 We estimate the extent of the outer shelf area with depositional conditions comparable
687 to those investigated here to cover approximately 280,000 km^2 of the Laptev Sea. For the East
688 Siberian Sea, we estimate the respective area of the outer shelf to be 340,000 km^2. Due to the
689 stronger terrestrial influence in the Laptev Sea, we calculated rates separately for the two shelf
690 seas. The areal coverage with sediment stations was too sparse for statistically significant
691 interpolations between stations that would give reliable spatial accounts of the gradients in
692 rates between the stations. Instead, arithmetic averages of sediment mineralization rates and
693 fluxes were calculated for these regions. Accepting the uncertainties in our assessment and
694 data density, we estimate that the calculated areal rates could deviate by up to 50%. Table 5
695 lists the calculated rates based on the average flux calculated per square meter per day for
696 oxygen uptake, DIC flux, bacterial sulfate, and total anaerobic carbon mineralization. For the
697 latter three methods, the total flux was calculated for the marine and terrestrial component,
698 respectively. The same analysis could not be performed for the oxygen uptake for the reasons
699 discussed in section 4.3. Since the major part of the oxygen uptake is likely associated with
700 degradation of a highly reactive marine organic carbon component, the proportions calculated
701 based on the $\delta^{13}C$ composition of DIC would not necessarily apply to the topmost mm of

sediment. It is noteworthy to say that the rates calculated with our data set agree well with the O_2 uptake rates recently published by Bourgeois et al. (2017) for the Laptev Sea. Our calculations suggest that 5.2 and 10.4 Tg O_2 y^{-1}, respectively are taken up by the outer shelf sediment in the Laptev and East Siberian Sea, respectively, totaling 15.9 Tg y^{-1} for the whole investigated area (Table 5). Anaerobic carbon mineralization based on DIC, ^{35}S-SRR and combined manganese, iron, and sulfate reduction range between 0.62 and 1.28 Tg y^{-1}. Of the total anaerobic carbon mineralization, between 0.25 and 0.48 Tg y^{-1} can be attributed to the oxidation of terrestrially derived organic material. This rate is five to ten times lower than the estimated annual water column degradation of particulate terrestrial organic matter in the Eastern Siberian Arctic shelf system of 2.5±1.6 Tg y^{-1} (Sanchez et al. 2011), and only between 0.5% and 2% of the annual organic carbon export from land (Stein and Macdonald, 2004; Vonk et al., 2012).

5. Conclusions

Directly measured carbon mineralization rates together with stable isotope and concentration data of East Siberian Arctic shelf and slope porewaters indicate that about one third of the remineralized organic carbon in porewater DIC is derived from terrestrial organic matter. This conclusion confirms and extends previous observations that terrestrial organic carbon buried in Siberian shelf and slope sediment is not conservative (Semiletov et al., 2013; Karlsson et al., 2015; Bröder et al., 2016b). While mineralization of terrestrial organic material was described for the water column and resuspended surface sediment, our data indicate that mineralization also proceeds long after burial in sediment. Area-integrated rates of carbon mineralization in the outer shelf sediments (0.25 to 0.48 Tg y^{-1}) represent about 0.5 % to 8 % of the annual terrestrial organic matter load to the Laptev and East Siberian Sea ranging from 6 Tg y^{-1} (Stein and Macdonald, 2004) to 22 ± 8 to 44 Tg y^{-1} (Vonk et al., 2012). There are large uncertainties associated with these estimates, given that our calculations do not account for carbon mineralization of resuspended terrestrial organic material and likely higher rates of mineralization in the inner shelf sediments. Nevertheless, these data indicate that the contribution of the benthic DIC flux to the total CO_2 production in the outer Eastern Siberian Sea and Laptev Sea is small. This conclusion, however, does not necessarily extend to the inner parts of the Laptev Sea and the western parts of the East Siberian Sea, where CO_2 supersaturation has been reported by Semiletov et al. (2012) and Pipko et al. (2011).

Anderson et al (2009) estimated a DIC excess of 10 Tg C by evaluating data from the Laptev and East Siberian Seas collected in the summer of 2008 and suggested that this excess was caused mainly by terrestrial organic matter decomposition. Their estimate can be compared to our sediment oxygen uptake for the outer Laptev and East Siberian Sea shelf of almost 16 Tg y^{-1}, which would demand that 62.5 % of the oxygen uptake was due to terrestrial organic matter mineralization. However, the reported annual production of marine organic matter for the total Laptev and East Siberian Sea is about 46 Tg y^{-1} (Stein and Macdonald, 2004). Even if only half of this amount is produced in the outer shelf region and only another half of that amount was deposited, there would still be more than 10 Tg y^{-1} of reactive marine organic matter at the sediment surface. Our data would therefore suggest that at least in the more productive East Siberian Sea the pronounced aragonite undersaturation reported for bottom waters in the East Siberian Sea is due to aerobic mineralization of a significant amount of marine organic matter. It is apparent that these sediments play a major role in the recycling of marine organic carbon on the Arctic shelf. Future changes in marine production on the Siberian shelf under longer ice-free conditions (Arrigo and van Dijken, 2011) will likely change the relative proportions of degrading marine and terrestrial organic matter further so that this particular shelf system may in the future more strongly resemble that of other ice-free shelf-slope environments.

6. Acknowledgements

Funding for this investigation came from the K&A Wallenberg foundation, the Swedish Polarsekretariat, and the Bolin Centre for Climate Research at Stockholm University. Igor Semiletov acknowledge support from the Russian Government (No. 14.Z50.31.0012/03.19.2014). We would like to thank the members of the SWERUS-C3 consortium, the shipcrew on icebreaker Oden, and Heike Siegmund, Lina Hansson, Barkas Charalampos, and Dimitra Panagiotopoulou for help with the laboratory work. We dedicate this publication to our friend and colleague Vladimir Samarkin, who unfortunately passed away before publication of this work. This manuscript benefitted from discussions with Patrick Crill, Rienk Smittenberg, Örjan Gustafsson, Christoph Humborg, Julia Steinbach, Clint Miller, Marc Geibel, Emma Karlsson, Brett Thornton, Jorien Vonk, Leif Anderson, and Magnus Mörth.

7. References

Alling, V., Sanchez-Garcia, L., Porcelli, D., Pugach, S., Vonk, J. E., van Dongen, B., Mörth, C.-M., Anderson, L. G., Sokolov, A., Andersson, P., Humborg, C., Semiletov, I., and Gustafsson, Ö.: Non-conservative behavior of dissolved organic carbon across the Laptev and East Siberian seas, Global Biogeochemical Cycles, 24, 10.1029/2010gb003834, 2010.

Alling, V., Porcelli, D., Mörth, C. M., Anderson, L. G., Sanchez-Garcia, L., Gustafsson, Ö., Andersson, P. S., and Humborg, C.: Degradation of terrestrial organic carbon, primary production and out-gassing of CO_2 in the Laptev and East Siberian Seas as inferred from $\delta^{13}C$ values of DIC, Geochimica et Cosmochimica Acta, 95, 143-159, 2012.

Anderson LG, Jutterström S, Hjalmarsson S, Wahlstrom I, Semiletov IP. Out-gassing of CO_2 from Siberian Shelf seas by terrestrial organic matter decomposition. Geophysical Research Letters, **36**, L20601, 2009.

Arrigo, K. R., and van Dijken, G. L.: Secular trends in Arctic Ocean net primary production, Journal of Geophysical Research: Oceans, 116, 10.1029/2011JC007151, 2011.

Bauch, D., Dmitrenko, I., Kirillov, S., Wegner, C., Hölemann, J., Pivovarov, S., Timokhov, L., and Kassens, H.: Eurasian Arctic shelf hydrography: Exchange and residence time of southern Laptev Sea waters, Continental Shelf Research, 29, 1815-1820, 2009.

Berg, P., Petersen-Risgaard, N., and Rysgaard, S.: Interpretation and measured concentration profiles in sediment pore water, Limnology and Oceanography, 43, 1500-1510, 1998.

Berg, P., Rysgaard, S., and Thamdrup, B.: Dynamic modeling of early diagenesis and nutrient cycling. A case study in an Arctic marine sediment, Amer. J. Sci, 303, 906-955, 2003.

Boetius, A., and Damm, E.: Benthic oxygen uptake, hydrolytic potentials and microbial biomass at the Arctic continental slope, Deep Sea Research Part I: Oceanographic Research Papers, 45, 239-275, 1998.

Boudreau, B. P.: Diagenetic models and their implementation, Springer Verlag, 414 pp., 1996.

Bourgeois, S., Archambault, P., and Witte, U.: Organic matter remineralization in marine sediments: A Pan-Arctic synthesis, Global Biogeochemical Cycles, 31, 190-213, 2017.

Bröder, L.-M., Tesi, T., Salvado, J. A., Semiletov, I., Dudarev, O. V., and Gustafsson, Ö.: Fate of terrigeneous organic matter across the Laptev Sea from the mouth of the Lena River to the deep sea of the Arctic interior, Biogeosciences, 13, 5003-5019, 2016a.

Bröder, L., Tesi, T., Andersson, A., Eglinton, T. I., Semiletov, I. P., Dudarev, O. V., Roos, P., and Gustafsson, Ö.: Historical records of organic matter supply and degradation status in the East Siberian Sea, Organic Geochemistry, 91, 16-30, 2016b.

Canfield, D. E., Kristensen, E., and Thamdrup, B.: Aquatic geomicrobiology, Advances in marine biology, 48, 2005.

Dmitrenko, I. A., Tyshko, K. N., Kirillov, S. A., Eicken, H., Hölemann, J. A., and Kassens, H.: Impact of flaw polynyas on the hydrography of the Laptev Sea, Global and Planetary Change, 48, 9-27, 2005.

Dmitrenko, I. A., Kirillov, S. A., and Tremblay, L. B.: The long-term and interannual variability of summer fresh water storage over the eastern Siberian shelf: Implication for climatic change, Journal of Geophysical Research: Oceans, 113, doi: 10.1029/2007JC004304, 2008.

Dudarev, O. V., Semiletov, I. P., and Charkin, A. N.: Particulate material composition in the Lena River-Laptev Sea system: Scales of heterogeneities. In: Doklady Earth Sciences, 6, 1000-1005, 2006.

Fahl, K., and Nöthig, E.-M.: Lithogenic and biogenic particle fluxes on the Lomonosov Ridge (central Arctic Ocean) and their relevance for sediment accumulation: Vertical vs. lateral transport, Deep Sea Research Part I: Oceanographic Research Papers, 54, 1256-1272, 2007.

Glud, R. N.: Oxygen dynamics of marine sediments, Mar. Biol. Res., 4, 243-289, 2008.

Grebmeier, J. M., Cooper, L. W., Feder, H. M., and Sirenko, B. I.: Ecosystem dynamics of the Pacific-influenced Northern Bering and Chukchi Seas in the Amerasian Arctic, Progress in Oceanography, 71, 331-361, 2006.

Guay, C. K., Falkner, K. K., Muench, R. D., Mensch, M., Frank, M., and Bayer, R.: Wind-driven transport pathways for Eurasian Arctic river discharge, Journal of Geophysical Research: Oceans, 106, 11469-11480, 2001.

Guo, L., Ping, C. L., and Macdonald, R. W.: Mobilization pathways of organic carbon from permafrost to arctic rivers in a changing climate, Geophysical Research Letters, 34, 2007.

Hall, P. O. J., and Aller, R. C.: Rapid, small-volume flow injection analysis for ΣCO_2 and NH_4^+ in marine and freshwaters, Limnology and Oceanography, 37, 1113-1119, 1992.

Hugelius, G., Strauss, J., Zubrzycki, S., Harden, J. W., Schuur, E. A. G., Ping, C. L., Schirrmeister, L., Grosse, G., Michaelson, G. J., Koven, C. D., O'Donnell, J. A., Elberling, B., Mishra, U., Camill, P., Yu, Z., Palmtag, J., and Kuhry, P.: Estimated stocks of circumpolar permafrost carbon with quantified uncertainty ranges and identified data gaps, Biogeosciences, 11, 6573-6593, 2014.

Ivanov, V. V. and Golovin, P. N.: Observations and modeling of dense water cascading from the northwestern Laptev Sea shelf, Journal of Geophysical Research: Oceans, 112, 2007.

Jørgensen, B. B.: A comparison of methods for the quantification of bacterial sulfate reduction in coastal marine sediments: I. Measurement with radiotracer techniques, Geomicrobiology Journal, 1, 11-27, 1978.

Jørgensen, B. B., and Kasten, S.: Sulfur and methane oxidation, in: Marine Geochemistry, Second Edition ed., edited by: Schulz, H. D., and Zabel, M., Springer Verlag, Berlin Heidelberg, 271-309, 2006.

Kallmeyer, J., Ferdelman, T. G., Weber, A., Fossing, H., and Jørgensen, B. B.: Evaluation of a cold chromium distillation procedure for recovering very small amounts of radiolabeled sulfide related to sulfate reduction measurements., Limnol. Oceanog. Methods, 2, 171-180, 2004.

Karlsson, E. S., Brüchert, V., Tesi, T., Charkin, A., Dudarev, O., Semiletov, I., and Gustafsson, Ö.: Contrasting regimes for organic matter degradation in the East Siberian Sea and the Laptev Sea assessed through microbial incubations and molecular markers, Marine Chemistry, 170, 11-22, 2015.

Koven, C. D., Lawrence, D. M., and Riley, W. J.: Permafrost carbon-climate feedback is sensitive to deep soil carbon decomposability but not deep soil nitrogen dynamics, Proceedings of the National Academies of Science, 112, 3752-3757, 2015.

Lalonde, K., Mucci, A., Ouellet, A., and Gelinas, Y.: Preservation of organic matter in sediments promoted by iron, Nature, 483, 198-200, 2012.

Li, Y.-H. and Gregory, S.: Diffusion of ions in sea water and in deep-sea sediments, Geochimica et Cosmochimica Acta, 88, 703-714, 1974.

Macdonald, R. W., and Gobeil, C.: Manganese Sources and Sinks in the Arctic Ocean with Reference to Periodic Enrichments in Basin Sediments, Aquatic Geochemistry, 18, 565-591, 2012.

Mackin, J. E., and Aller, R.C.: Ammonium adsorption in marine sediments, Limnology and Oceanography, 29, 250-257, 1984.

Macdonald, R. W., Kuzyk, Z. Z. A., and Johannessen, S. C.: The vulnerability of Arctic shelf sediments to climate change, Environmental Reviews, 1-19, 2015.

McGuire, A. D., Anderson, L. G., Christensen, T. R., Dallimore, S., Guo, L., Hayes, D. J., Heimann, M., Lorenson, T. D., Macdonald, R. W., and Roulet, N.: Sensitivity of the carbon cycle in the Arctic to climate change, Ecological Monographs, 79, 523-555, 2009.

McTigue, N., Gardner, W., Dunton, K., and Hardison, A.: Biotic and abiotic controls on co-occurring nitrogen cycling processes in shallow Arctic shelf sediments, Nature Communications, 7, 2016.

Miller, C. M., Dickens, G. R., Jakobsson, M., Johansson, C., Koshurnikov, A., O'Regan, M., Muschitiello, F., Stranne, C., and Mörth, C.-M.: Low methane concentrations in sediment along the continental slope north of Siberia: Inference from pore water geochemistry, Biogeosciences Discussions, doi:10.5194/bg-2016-308, 2016.

Naidu, A. S., Cooper, L. W., Finney, B. P., Macdonald, R. W., Alexander, C., and Semiletov, I. P.: Organic carbon isotope ratios ($\delta^{13}C$) of Arctic Amerasian Continental shelf sediments. International Journal of Earth Sciences, 89, 522-532, 2000.

Nickel, M., Vandieken, V., Brüchert, V., and Jørgensen, B. B.: Microbial Mn(IV) and Fe(III) reduction in northern Barents Sea sediments under different conditions of ice cover and

877 organic carbon deposition, Deep Sea Research Part II: Topical Studies in Oceanography, 55,
878 2390-2398, 2008.

879 Nitishinsky, M., Anderson, L. G., and Hölemann, J. A.: Inorganic carbon and nutrient fluxes
880 on the Arctic Shelf, Continental Shelf Research, 27, 1584-1599, 2007.

881 Pipko, I., Semiletov I.P., Pugach S.P., Wahlstrom I., Anderson L.G. Interannual variability of
882 air-sea CO_2 fluxes and carbon system in the East Siberian Sea. Biogeosciences, **8**, 1987-2007,
883 2011.

884 Pivovarov, S., Hölemann, J., Kassens, H., Antonow, M., and Dmitrenko, I.: Dissolved
885 oxygen,silicon,phosphorous and suspended matter concentrations during the spring breakup
886 of the Lena River, in: Land–Ocean Systems in the Siberian Arctic:Dynamics and History,
887 edited by: Kassens, H., Bauch, H. A., Dmitrenko, I., Eicken, H., Hubberten, H.-W., Melles,
888 M., Thiede, J., and Timokhov, L., Springer, Berlin, 251-264, 1999.

889 Qi, D., Chen, L., Chen, B., Gao, Z., Zhong, W., Feely, R. A., Anderson, L. G., Sun, H., Chen,
890 J., Chen, M., Zhan, L., Zhang, Y., and Cai, W.-J.: Increase in acidifying water in the western
891 Arctic Ocean, Nature Clim. Change, 7, 195-199, 2017.

892 Rachold, V., Eicken, H., Gordeev, V., Grigoriev, M. N., Hubberten, H.-W., Lisitzin, A. P.,
893 Shevchenko, V., and Schirrmeister, L.: Modern terrigenous organic carbon input to the Arctic
894 Ocean, in: The organic carbon cycle in the Arctic Ocean, Springer, 33-55, 2004.

895 Rasmussen, H., and Jørgensen, B. B.: Microelectrode studies of seasonal oxygen uptake in a
896 coastal sediment: Role of molecular diffusion, Marine ecology progress series. Oldendorf, 81,
897 289-303, 1992.

898 Raymond, P. A., McClelland, J., Holmes, R., Zhulidov, A., Mull, K., Peterson, B., Striegl, R.,
899 Aiken, G., and Gurtovaya, T.: Flux and age of dissolved organic carbon exported to the Arctic
900 Ocean: A carbon isotopic study of the five largest arctic rivers, Global Biogeochemical
901 Cycles, 21, 10.1029/2007GB002983, 2007.

902 Rekant, P., Bauch, H. A., Schwenk, T., Portnov, A., Gusev, E., Spiess, V., Cherkashov, G.,
903 and Kassens, H.: Evolution of subsea permafrost landscapes in Arctic Siberia since the Late
904 Pleistocene: a synoptic insight from acoustic data of the Laptev Sea, Arktos, 1,
905 10.1007/s41063-015-0011-y, 2015.

Rossel, P. E., Bienhold, C., Boetius, A., and Dittmar, T.: Dissolved organic matter in pore water of Arctic Ocean sediments: Environmental influence on molecular composition, Organic Geochemistry, 97, 41-52, 2016.

Sakshaug, E.: Primary and secondary production in the Arctic Seas, in: The organic carbon cycle in the Arctic Ocean, Springer, 57-81, 2004.

Salvadó, J. A., Tesi, T., Andersson, A., Ingri, J., Dudarev, O. V., Semiletov, I. P., and Gustafsson, Ö.: Organic carbon remobilized from thawing permafrost is resequestered by reactive iron on the Eurasian Arctic Shelf, Geophysical Research Letters, 42, 8122-8130, 2015.

Sánchez-García, L., Alling, V., Pugach, S., Vonk, J., van Dongen, B., Humborg, C., Dudarev, O., Semiletov, I., and Gustafsson, Ö.: Inventories and behavior of particulate organic carbon in the Laptev and East Siberian seas, Global Biogeochemical Cycles, 25, 10.1029/2010gb003862, 2011.

Savvichev, A., Rusanov, I., Pimenov, N., Zakharova, E., Veslopolova, E., Lein, A. Y., Crane, K., and Ivanov, M.: Microbial processes of the carbon and sulfur cycles in the Chukchi Sea, Microbiology, 76, 603-613, 2007.

Schuur, E. A. G., McGuire, A. D., Schadel, C., Grosse, G., Harden, J. W., Hayes, D. J., Hugelius, G., Koven, C. D., Kuhry, P., Lawrence, D. M., Natali, S. M., Olefeldt, D., Romanovsky, V. E., Schaefer, K., Turetsky, M. R., Treat, C. C., and Vonk, J. E.: Climate change and the permafrost carbon feedback, Nature, 520, 171-179, 2015.

Seeberg-Elverfeldt, J., Schlüter, M., Feseker, T., and Kölling, M.: Rhizon sampling of porewaters near the sediment-water interface of aquatic systems, Limnol. Oceanogr. Methods, 3, 361-371, 2005.

Semiletov, I., Dudarev, O., Luchin, V., Charkin, A., Shin, K.-H., and Tanaka, N.: The East Siberian Sea as a transition zone between Pacific-derived waters and Arctic shelf waters, Geophysical Research Letters, 10.1029/2005GL022490, 2005.

Semiletov, I., Pipko, I., Gustafsson, Ö., Anderson, L. G., Sergienko, V., Pugach, S., Dudarev, O., Charkin, A., Gukov, A., Broder, L., Andersson, A., Spivak, E., and Shakhova, N.: Acidification of East Siberian Arctic Shelf waters through addition of freshwater and terrestrial carbon, Nature Geoscience, 9, 361-365, 2016.

936 Semiletov I.P., Shakhova, N.E, Pipko, I.I.: Space-time dynamics of carbon and environmental
937 parameters related to carbon dioxide emissions in the Buor-Khaya Bay and adjacent part of
938 the Laptev Sea. Biogeosciences, **10**, 5977-5996, 2013.

939 Semiletov I.P., Pipko I.I., Shakhova N.E., Dudarev O.V., Pugach S.P., Charkin A.N., McRoy
940 C.P., Kosmach D., and Ö. Gustafsson.: Carbon transport by the Lena River from its
941 headwaters to the Arctic Ocean, with emphasis on fluvial input of terrestrial particulate
942 organic carbon vs. carbon transport by coastal erosion. Biogeosciences, **8**, 2407-2426, 2011.

943 Semiletov, I.P., Destruction of the coastal permafrost ground as an important factor in
944 biogeochemistry of the Arctic Shelf waters, Trans. (Doklady) Russian Acad. Sci., 368, 679-
945 682, 1999 (translated into English).

946 Stein, R., and Macdonald, R. W.: The Organic Carbon Cycle in the Arctic Ocean, Springer-
947 Verlag, Berlin, 382 pp., 2004.

948 Strobl, C., Schulz, V., Vogler, S., Baumann, S., Kassens, H., Kubik, P. W., Suter, M., and
949 Mangini, A.: Determination of depositional beryllium-10 fluxes in the area of the Laptev Sea
950 and beryllium-10 concentrations in water samples of high northern latitudes, in: Land-Ocean
951 Systems in the Siberian Arctic: Dynamics and History, edited by: Kassens, H., Bauch, H. A.,
952 Dmitrenko, I., Eicken, H., Hubberten, H.-W., Melles, M., Thiede, J., and Timokhov, L.,
953 Springer, Berlin, 515-532, 1998.

954 Tarnocai, C., Canadell, J. G., Schuur, E. A. G., Kuhry, P., Mazhitova, G., and Zimov, S.: Soil
955 organic carbon pools in the northern circumpolar permafrost region, Global Biogeochemical
956 Cycles, 23, 10.1029/2008gb003327, 2009.

957 Tesi, T., Semiletov, I., Hugelius, G., Dudarev, O., Kuhry, P., and Gustafsson, Ö.:
958 Composition and fate of terrigenous organic matter along the Arctic land–ocean continuum in
959 East Siberia: Insights from biomarkers and carbon isotopes, Geochimica et Cosmochimica
960 Acta, 133, 235-256, 2014.

961 Tesi, T., Semiletov, I., Dudarev, O., Andersson, A., and Gustafsson, Ö.: Matrix association
962 effects on hydrodynamic sorting and degradation of terrestrial organic matter during cross-
963 shelf transport in the Laptev and East Siberian shelf seas, Journal of Geophysical Research:
964 Biogeosciences, 121, 731-752, 2016.

965 Tesi, T., Geibel, M. C., Pearce, C., Panova, E., Vonk, J. E., Karlsson, E., Salvado, J. A.,
966 Kruså, M., Bröder, L., Humborg, C., Semiletov, I., and Gustafsson, Ö.: Carbon geochemistry
967 of plankton-dominated samples in the Laptev and East Siberian shelves: contrasts in
968 suspended particle composition, Ocean Sci., 13, 735-748, 10.5194/os-13-735-2017, 2017.

969 Thamdrup, B.: Bacterial manganese and iron reduction in aquatic sediments, Advances in
970 Microbial Ecology, 16, 41-84, 2000.

971 Arrigo, K. R., and van Dijken, G. L.: Secular trends in Arctic Ocean net primary production,
972 Journal of Geophysical Research: Oceans, 116, 10.1029/2011JC007151, 2011.

973 Hugelius, G., Strauss, J., Zubrzycki, S., Harden, J. W., Schuur, E. A. G., Ping, C. L.,
974 Schirrmeister, L., Grosse, G., Michaelson, G. J., Koven, C. D., O'Donnell, J. A., Elberling, B.,
975 Mishra, U., Camill, P., Yu, Z., Palmtag, J., and Kuhry, P.: Estimated stocks of circumpolar
976 permafrost carbon with quantified uncertainty ranges and identified data gaps,
977 Biogeosciences, 11, 6573-6593, 2014.

978 Qi, D., Chen, L., Chen, B., Gao, Z., Zhong, W., Feely, R. A., Anderson, L. G., Sun, H., Chen,
979 J., Chen, M., Zhan, L., Zhang, Y., and Cai, W.-J.: Increase in acidifying water in the western
980 Arctic Ocean, Nature Clim. Change, 7, 195-199, 2017.

981 Sánchez-García, L., Alling, V., Pugach, S., Vonk, J., van Dongen, B., Humborg, C., Dudarev,
982 O., Semiletov, I., and Gustafsson, Ö.: Inventories and behavior of particulate organic carbon
983 in the Laptev and East Siberian seas, Global Biogeochemical Cycles, 25,
984 10.1029/2010gb003862, 2011.

985 Vandieken, V., Nickel, M., and Jørgensen, B. B.: Carbon mineralization in Arctic sediments
986 northeast of Svalbard: (Mn(IV) and Fe(III) reduction as principal anaerobic respiratory
987 pathways, Marine Ecology Progress Series, 322, 15-27, 2006.

988 Vonk, J. E., Sanchez-Garcia, L., van Dongen, B. E., Alling, V., Kosmach, D., Charkin, A.,
989 Semiletov, I. P., Dudarev, O. V., Shakhova, N., Roos, P., Eglinton, T. I., Andersson, A., and
990 Gustafsson, O.: Activation of old carbon by erosion of coastal and subsea permafrost in Arctic
991 Siberia, Nature, 489, 137-140.

992 Wegner, C., Hölemann, J. A., Dmitrenko, I., Kirillov, S., and Kassens, H.: Seasonal variations
993 in Arctic sediment dynamics—evidence from 1-year records in the Laptev Sea (Siberian
994 Arctic), Global and Planetary Change, 48, 126-140, 2005.

995 Wegner, C., Bauch, D., Hölemann, J. A., Janout, M. A., Heim, B., Novikhin, A., Kassens, H.,
996 and Timokhov, L.: Interannual variability of surface and bottom sediment transport on the
997 Laptev Sea shelf during summer, Biogeosciences, 10, 1117-1129, 2013.

998 Weingartner, T. J., Danielson, S., Sasaki, Y., Pavlov, V., and Kulakov, M.: The Siberian
999 Coastal Current: A wind- and buoyancy-forced Arctic coastal current, Journal of Geophysical
1000 Research: Oceans, 104, 29697-29713, 1999.

1001

List of Tables

List of figures

Fig. 8 A. Map of field area and sampling stations showing oxygen uptake rates. For comparison, oxygen uptake rates reported in Boetius and Damm (1998) are shown as triangles using the same color code. B: Map of field area and sampling stations with depth-integrated sulfate reduction rates.

Fig. 9 A. Water depth variation of sediment oxygen uptake. B: Water depth variation of integrated ^{35}S-sulfate reduction rates (0-30 cm sediment depth). For reference average rates of abyssal plain, continental rise, slope, and shelf sediments, deposition and non-depositional, are shown for reference.

Table 1. Physical and chemical characteristics of sediment and bottom water at the sampled stations

Station	Latitude °N	Longitude °E	Date	Water depth	Ice cover	Bottom water salinity	Bottom water temperature	Bottom water O_2 concentration	Bottom water NH_4^+ concentration	Bottom water DIC above sediment	$\delta^{13}C$ DIC bottom water	$\delta^{13}C$ surface sediment org C (Salvado et al. (2017)	Sediment description
			Month/Day/Year	m	%	‰	°C	µmol/L	µmol/L	µmol/L	‰ vs. VPDB	‰ vs. VPDB	
1	78.942	125.243	7/15/2014	3146	50 - 75	34.9	-0.9	271.9	1.65	2151.5	-0.5	-22.3	clay, brown
2	78.581	125.607	7/16/2014	2900	25 - 50	34.9	-0.9	275.0	n.a.	n.a.	n.a.	n.a.	clay, brown
3	78.238	126.150	7/16/2014	2601	< 25	34.9	-0.9	280.0	n.a.	n.a.	n.a.	n.a.	clay, brown
4	77.855	126.664	7/16/2014	2106	< 25	34.9	-0.8	289.4	1.81	2164.5	-1.6	-22.5	clay, brown
6	77.142	127.378	7/17/2014	89	0.0	34.6	-1.8	327.0	1.30	2213.0	-2.2	-23.2	clay, top 3 cm brown, then gray, fauna on top of sediment
23	76.171	129.333	7/22/2014	56	0.0	34.2	-1.8	303.2	1.34	2246.3	-3.2	-25.0	silty clay, top 4 cm brown, then gray, brittle stars
24	75.599	129.558	7/24/2014	46	0.0	34.0	-1.7	283.8	0.89	2244.1	-2.0	-24.8	silty clay, top 4 cm brown, then gray
27	76.943	132.229	7/23/2014	44	0.0	34.2	-1.8	332.3	0.94	2595.0	-6.5	-24.2	silty clay, top 2 cm brown, then gray, fluffy surface layer, brittle stars
30	78.181	138.354	7/24/2014	69	0.0	34.1	-1.6	334.8	0.79	2178.4	-3.7	-23.4	silty clay, top 4 cm brown, then gray
31	79.396	135.497	7/25/2014	3056	0.0	34.9	-0.9	270.9	0.74	2161.7	n.a.	n.a.	clay, brown
35	78.600	137.061	7/26/2014	541	0.0	34.9	0.4	288.1	0.43	2183.7	n.a.	n.a.	clay top 15cm brown, fluffy, inhomogeneous, surface-dwelling fauna
37	78.521	137.170	7/26/2014	205	0.0	34.7	0.0	295.4	0.89	2171.1	n.a.	n.a.	clay, top 5cm brown, then gray
40	77.670	144.668	7/27/2014	45	0.0	31.5	-1.3	190.3	0.53	2213.7	-1.6	-23.7	silty clay, top 3cm brown, then gray, brittle stars
43	76.780	147.791	7/28/2014	42	25-50	30.1	-1.2	256.4	0.61	2086.7	n.a.	n.a.	silty clay to clayey silt, top 2cm brown, then gray, some small durface-dwelling animals
45	76.416	148.115	7/29/2014	40	< 50	29.1	-1.3	319.9	0.57	2576.0	-2.1	-24.4	silty clay to clayey silt, 2cm brown, then gray-black, rather stiff
48	76.615	153.345	7/30/2014	49	> 75	30.6	-1.6	315.9	0.50	2075.1	-2.2	-25.8	silty clay to clayey silt, top 3cm brown, then grayblack
50	75.764	158.529	8/1/2014	44	> 75	31.1	-1.4	311.0	0.51	2068.7	-2.1	-24.6	silty clay to clayet silt, top 2cm brown, then grayblack
53	74.957	161.088	8/2/2014	47	> 75	31.0	-1.6	253.3	0.16	2086.1	-2.5	n.a.	silty clay to clayey silt, top 3 cm brown, then 3 cm gray, then grayblack
58	74.440	166.050	8/4/2014	54	> 75	31.4	-1.7	254.3	0.65	2154.9	-1.5	-23.8	silty clay to clayey silt, slightly resuspended, top 2 cm brown, then gray, soft
63	74.685	172.361	8/7/2014	67	> 75	32.4	-1.4	186.0	0.61	2240.8	-2.2	-22.7	silty clay to clayey silt, top 1cm brown, then gray

1054

Table 2. O_2 uptake, integrated ^{35}S-sulfate reduction rates, DIC flux, and porewater DIC/NH_4^+ ratios

Station	Water depth	mean O_2 penetration depth	mean O_2 at 60mm depth	O_2 uptake (modelled/measured with 2D optode)	^{35}S-SRR (0-30 cm) duplicates	DIC flux (modelled in anaerobic zone/measured with whole core incubation)	Average porewater DIC/NH_4^+
	m	mm	µmol/L	mmol m^{-2} d^{-1}	mmol m^{-2} d^{-1}	mmol m^{-2} d^{-1}	
1	3146	> 60	217	1.48 ± 0.08	0.05 / 0.21	-0.11	
2	2900	> 60	213	1.32 ± 0.05			
3	2601	> 60	194	0.81 ± 0.06			
4	2106	> 60	89	1.32 ± 0.05	0.17 / 0.17	-0.15	
6	89	36	0	2.61 ± 0.01	0.03 / 0.05	-0.08	
23	56	13	0	5.00 ± 0.09 ; 5.3 ± 0.2	0.56	-0.12; -5.1 ± 0.4	13
24	46	10	0	7.95 ± 0.14		-0.22	10
27	44	16	0	3.75 ± 0.08	0.37 / 0.20	-0.27	12
30	69	16	0	2.61 ± 0.11	0.06 / 0.03	-0.12	15
31	3056	> 60	194	1.78 ± 0.07			
35	541	> 60	30	2.43 ± 0.32			
37	205	44	0	2.51 ± 0.10			
Average Laptev Sea shelf				**4.20**	**0.19**	**0.2 ; 5.1**	**12**
40	45	12	0	4.62 ± 0.08	0.33 / 0.24	-0.19	16
43	42	13	0	4.7 ± 0.10			
45	40	10	0	4.02 ± 0.10	0.23 / 0.19	-0.37	13
48	49	5	0	9.14 ± 0.22	0.68 / 0.53	-0.71	10
50	44	9	0	5.65 ± 0.43; 5.2 ± 0.1	1.32 / 1.40	-1.01 ; -5.2 ± 0.2	12
53	47	10	0	4.53 ± 0.08 ; 4.7 ± 0.1	0.10 / 0.17	-0.20	14
58	54	3	0	11.49 ± 0.52	1.01	-1.27	24
63	67	4	0	10.72 ± 0.15 ; 10.8 ± 0.3	1.41	-1.35 ; -10.8 ± 0.6	12
Average East Siberian Sea shelf				**7.2**		**0.7 ; 8.0**	**14**

1055

1056

1057

Table 3. Anaerobic rates of carbon mineralization by manganese, iron, and sulfate reduction

	Net Fe^{2+} production	Net Mn^{2+} production	C-equivalent Fe + Mn reduction	^{35}S-Sulfate reduction	C-equivalents total anaerobic mineralization	Oxygen uptake	% Fe + Mn reduction of total anaerobic	Percentage anaerobic C mineralization of total	Percentage Fe and Mn mineralization of total
	mmol m^{-1} d^{-1}						%		
Station 23	0.05	0.03	0.03	0.56	1.1	5.0	2.3	22.9	0.5
Station 30	0.02	0.04	0.03	0.05	0.1	2.6	21.9	4.4	1.0
Station 45	0.14	0.12	0.09	0.21	0.5	4.0	18.3	12.8	2.3
Station 53	0.15	0.09	0.08	0.14	0.4	4.5	23.7	7.8	1.8
Station 63	-	0.50	0.25	1.41	3.1	10.7	8.1	26.0	2.3

1060

Table 4. Calculated carbon isotope composition of remineralized DIC and mass fractions of the marine and terrestrial endmembers and corresponding terrestrial carbon degradation rates based on ^{35}S-SRR and DIC flux

Station	Average $\delta^{13}C_{DIC}$ remineralized	Marine end member	Terrestrial end member	^{35}S-SRR-based terrestrial degradation rate	DIC-based terrestrial degradation rate
	‰ vs. VPDB	Mass fraction		mmol m^{-2} d^{-1}	mmol m^{-2} d^{-1}
1	-35.8	0.0	1.0	0.13	0.11
4	-24.7	0.73	0.27	0.05	0.04
6	-25.1	0.65	0.35	0.01	0.03
23	-24.5	0.78	0.22	0.12	0.03
24	-24.7	0.73	0.27		0.06
27	-25.4	0.58	0.42	0.12	0.11
30	-28.5	0.00	1.00	0.05	0.13
Average Laptev Sea shelf	**-25.6**	**0.53**	**0.47**	**0.08**	**0.07**
40	-21.4	0.72	0.28	0.08	0.05
45	-22.2	0.63	0.37	0.08	0.14
48	-23.0	0.54	0.46	0.28	0.32
50	-24.0	0.43	0.57	0.77	0.57
53	-18.8	1.00	0.00	0.00	0.00
58	-22.6	0.59	0.41	0.42	0.53
63	-20.3	0.84	0.16	0.25	0.22
Average East Siberian Sea shelf	**-21.8**	**0.68**	**0.32**	**0.27**	**0.26**

1061

Table 5. Regional estimates of sediment carbon mineralization in the outer Laptev and East Siberian shelf sea							
			Dissolved O_2 uptake	Upward DIC flux (anaerobic)	Terrestrial OC-derived DIC flux (anaerobic)	Marine OC-derived DIC flux (anaerobic)	Depth-integrated ^{35}S-SRR (C equivalent)
Outer Laptev Sea	Average	mmol m^{-2} d^{-1}	4.2	0.16	0.07	0.09	0.09
Outer East Siberian Sea	Average	mmol m^{-2} d^{-1}	7.2	0.73	0.26	0.47	0.34
Outer Laptev Sea	280,000 km^2	Tg C y^{-1}	5.2	0.20	0.09	0.11	0.11
Outer East Siberian Sea	340,000 km^2	Tg C y^{-1}	10.8	1.09	0.39	0.70	0.50
Total outer shelf area	620,000 km^2	Tg C y^{-1}	15.9	1.28	0.48	0.81	0.62
			^{35}S-SRR-based terrestrial C degradation	^{35}S-SRR-based marine C degradation	Total TEAP-based anaerobic OC degradation rate	Total TEAP-based anaerobic terrestrial OC degradation rate	Total TEAP-based anaerobic marine OC degradation rate
Outer Laptev Sea	Average	mmol m^{-2} d^{-1}	0.04	0.05	0.15	0.05	0.10
Outer East Siberian Sea	Average	mmol m^{-2} d^{-1}	0.13	0.21	0.42	0.16	0.26
Outer Laptev Sea	280,000 km^2	Tg C y^{-1}	0.05	0.07	0.18	0.06	0.12
Outer East Siberian Sea	340,000 km^2	Tg C y^{-1}	0.20	0.31	0.62	0.23	0.39
Total outer shelf area	620,000 km^2	Tg C y^{-1}	0.25	0.37	0.80	0.29	0.51

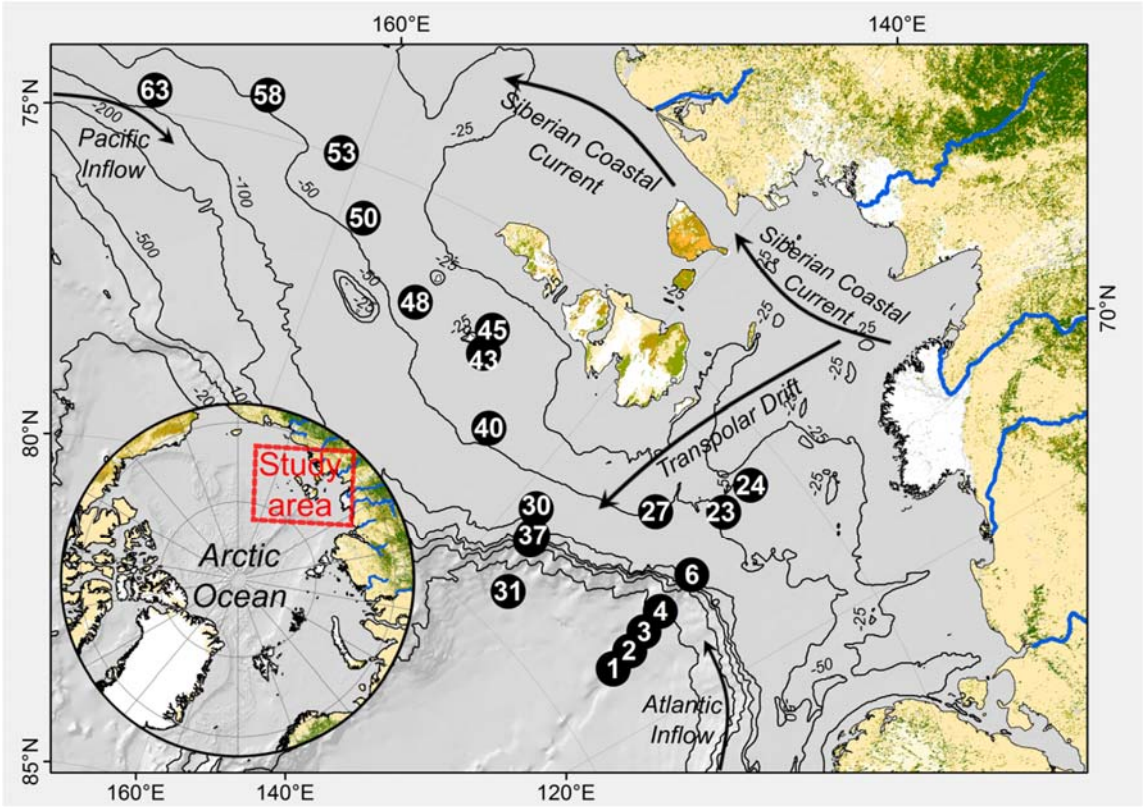

1063

1064 Fig. 1. Map of the Eastern Siberian Sea and slope and station locations.

1065

1066

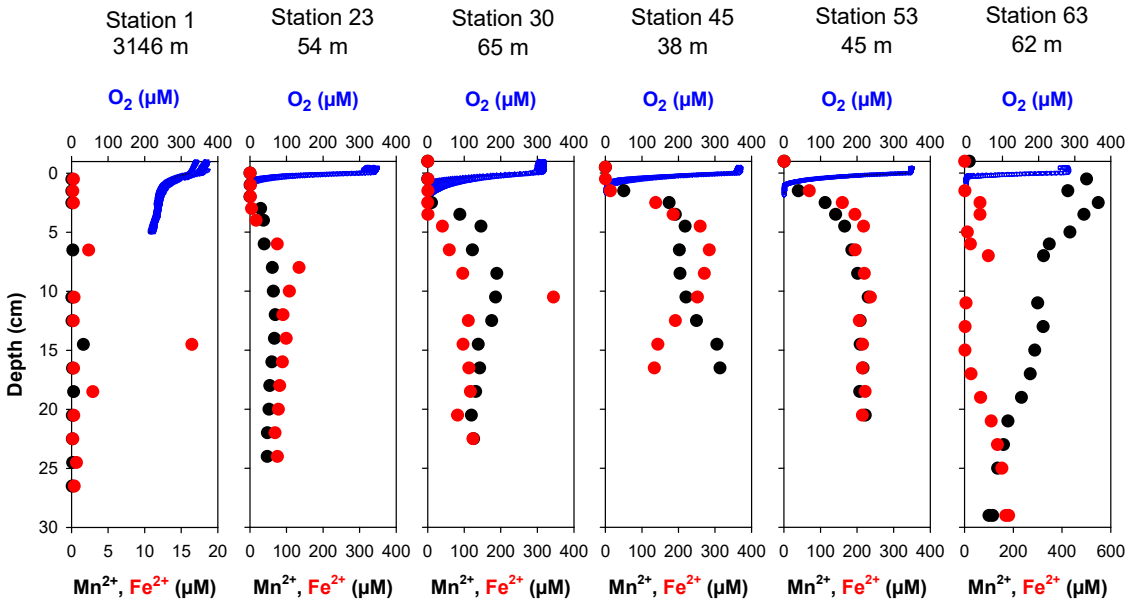

1067

1068 Fig. 2. Depth profiles of dissolved O_2, Fe^{2+}, and Mn^{2+} at Stations 1, 23, 30, 45, 53, and 63. For
1069 microelectrode profiles, 4 replicates are shown for each station. Depth resolution of measurement
1070 for O_2 was 100 µm.

1071

1072

1073

1074

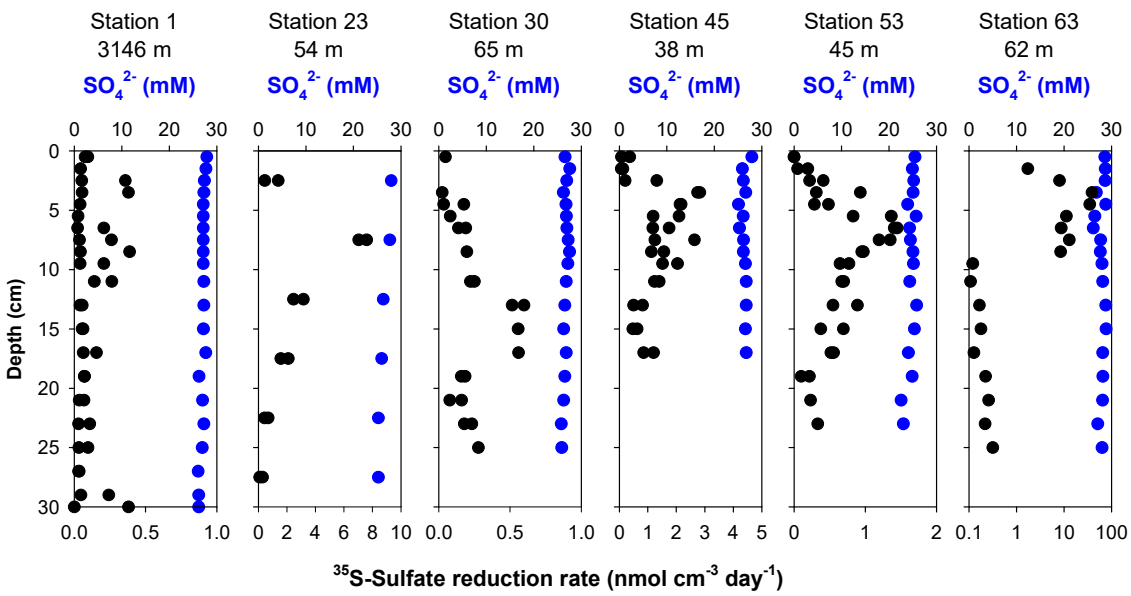

1075

1076 Fig. 3. Depth of profiles of ^{35}S-sulfate reduction rates and porewater concentration of dissolved
1077 sulfate for Stations 1, 23, 30, 45, 53, and 63. A replicate incubation was conducted for each depth
1078 except for Station 63.

1079

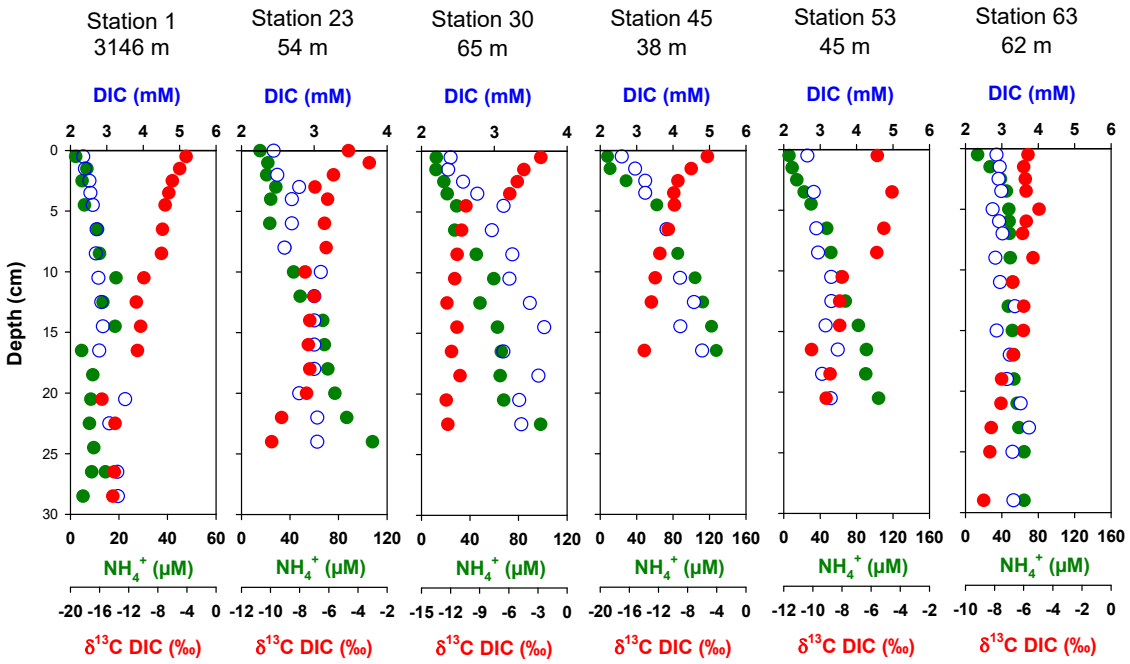

Fig. 4. Depth profiles of porewater dissovled inorganic carbon (DIC), $\delta^{13}C$ DIC and porewater NH_4^+ at stations 1, 23, 30, 45, 53, and 63.

1085

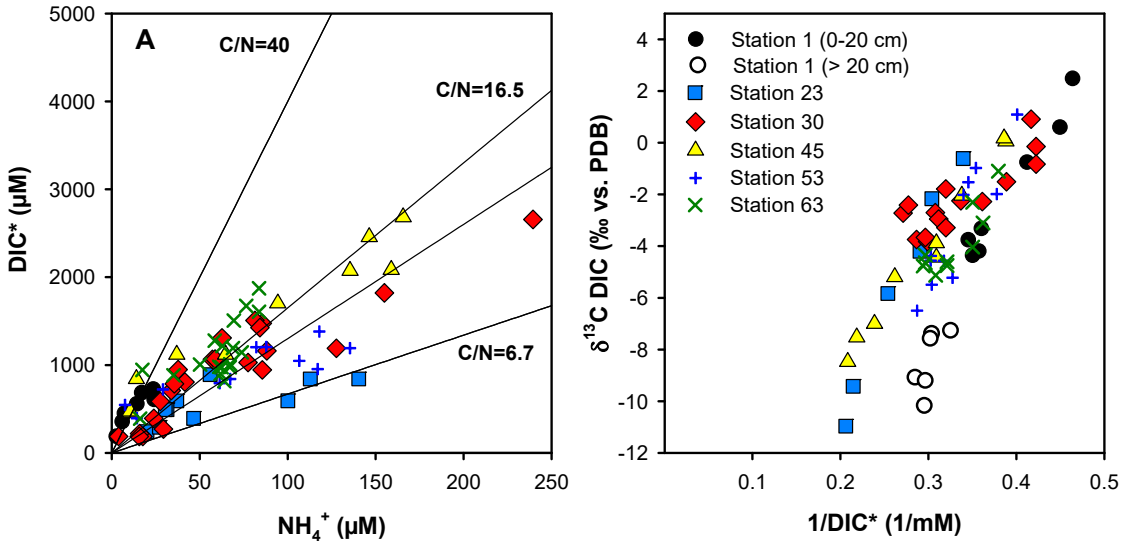

1086

1087 Fig. 5. A: Crossplot of dissolved NH_4^+ and porewater DIC* after correction for bottom water DIC
1088 concentrations. The slopes of the regression lines for the individual stations are shown in Table 2. B:
1089 Keeling plot of the fraction of remineralized DIC calculated from a 2-endmember mixing model
1090 versus $\delta^{13}C$ DIC.

1091

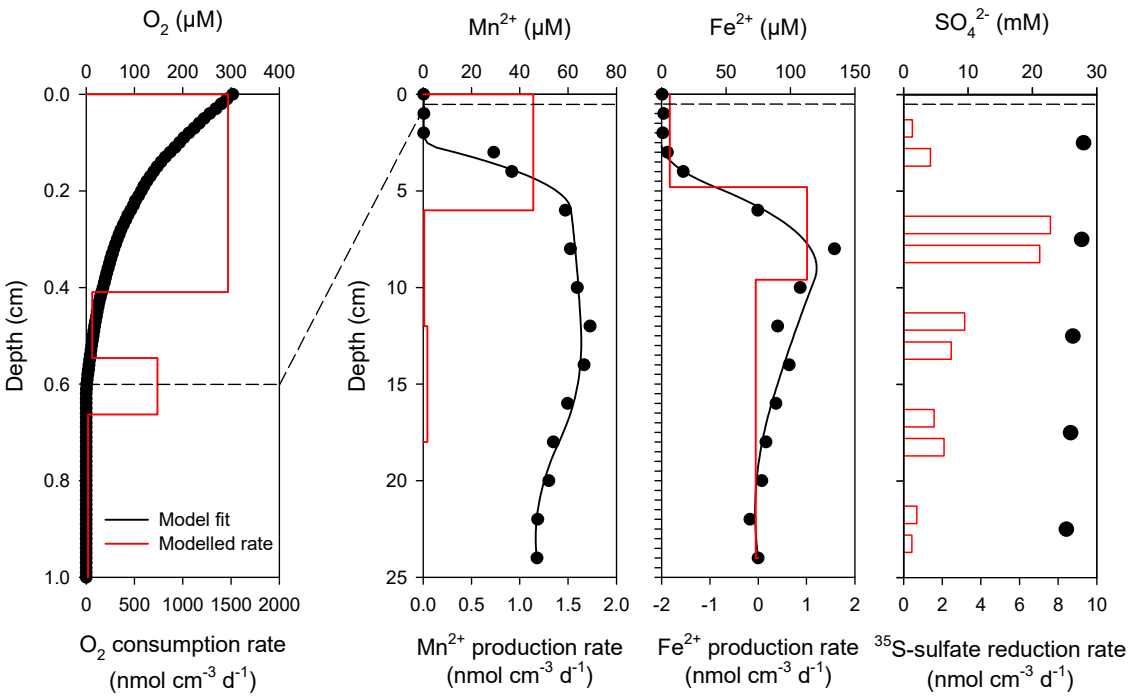

Fig. 6. Comparison of reaction rates of oxygen, manganese, iron, and sulfate reduction at Station 23. Note the different depth scale for the O_2 consumption rate. The dashed line marks the oxygen penetration depth.

1098

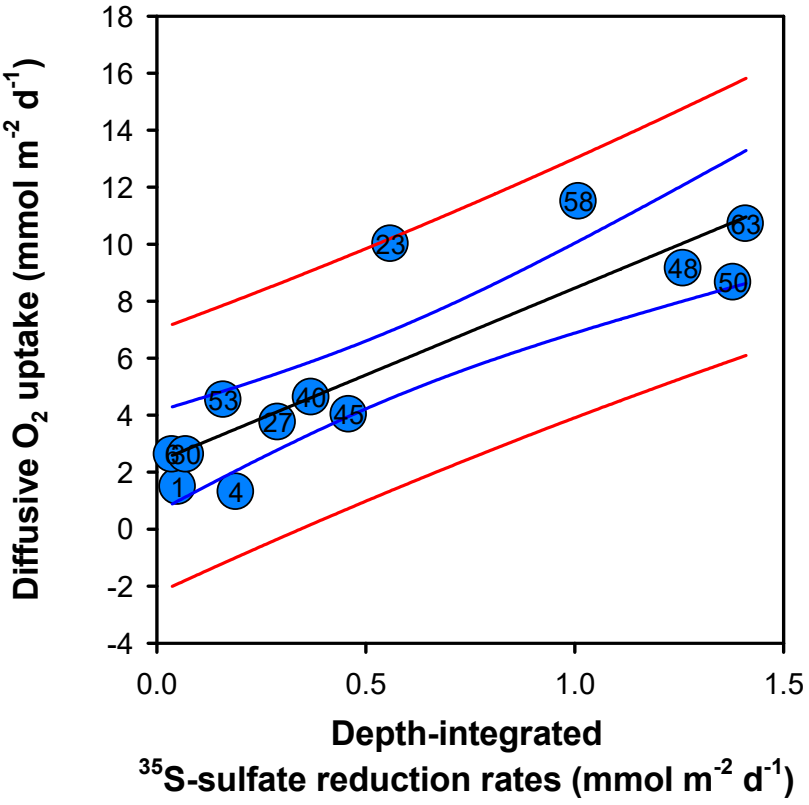

1099

1100 Fig. 7. Crossplot of diffusive oxygen uptake and integrated sulfate reduction rates. The black line is
1101 the linear regression and yielded a y-intercept of 2.1 mmol m^{-2} d^{-1} and a slope of 6.1 ± 0.1. Blue and
1102 red lines show the 95% and 99% confidence interval.

1103

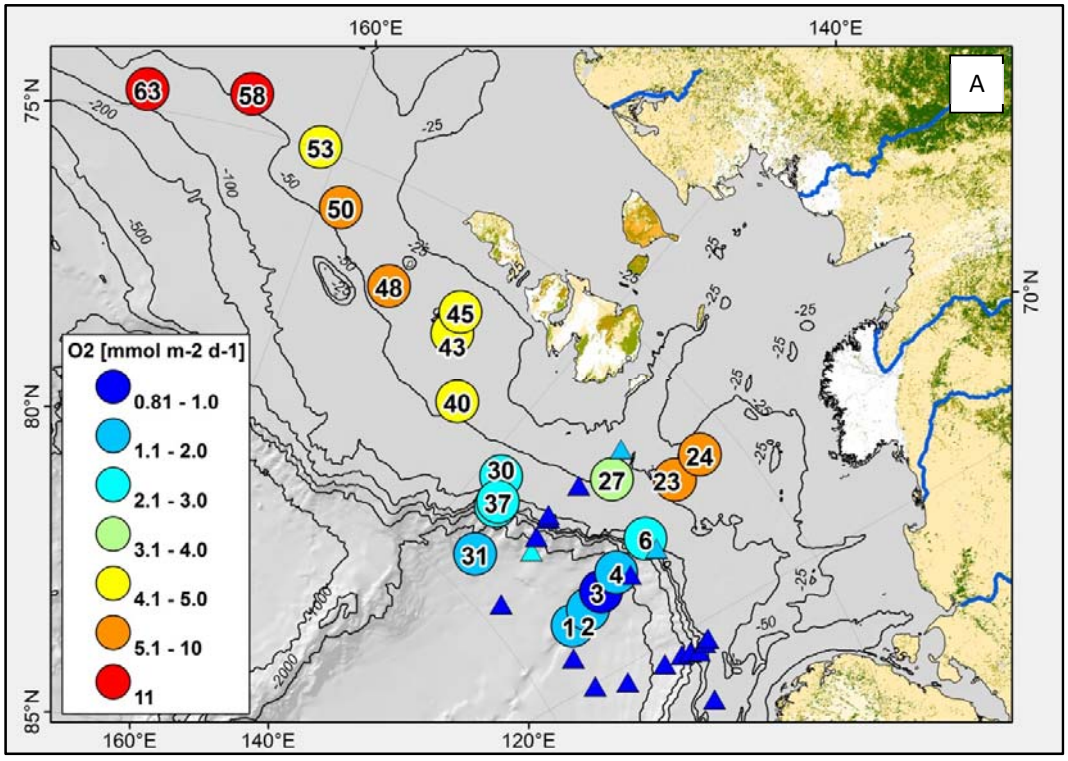

1104

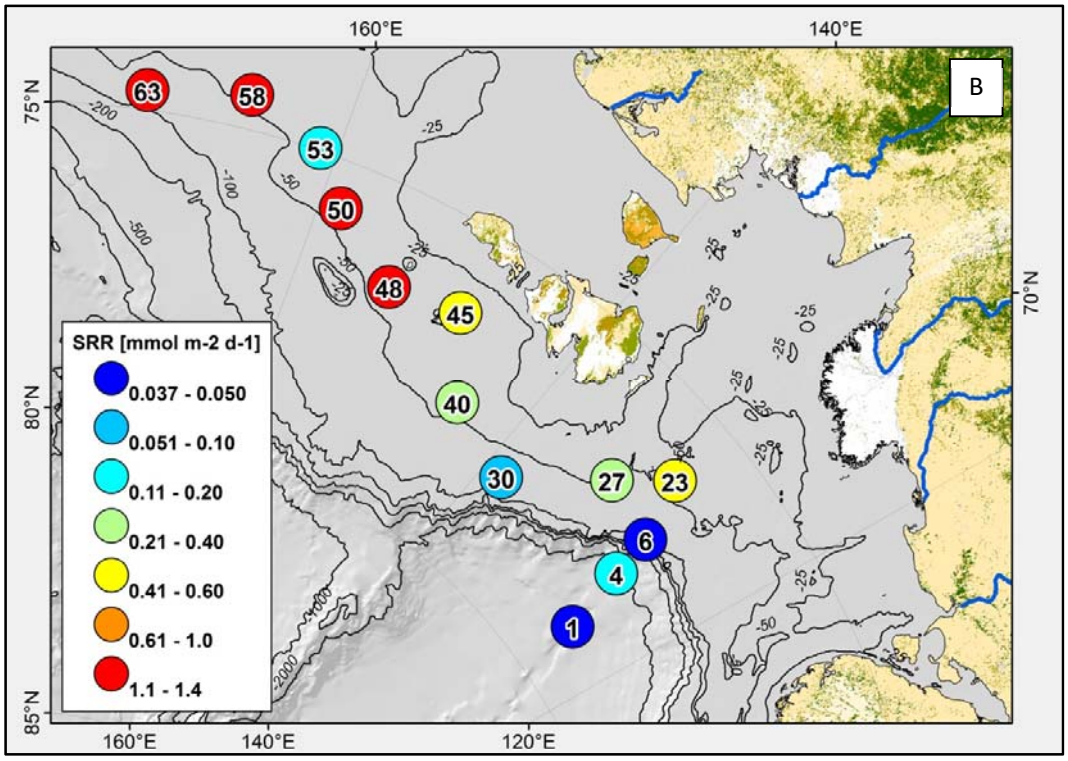

1105

1106 Fig. 8 A, B. Map of field area and sampling stations showing oxygen uptake rates in panel A and
1107 depth-integrated sulfate reduction rates in panel B.

1108

1109

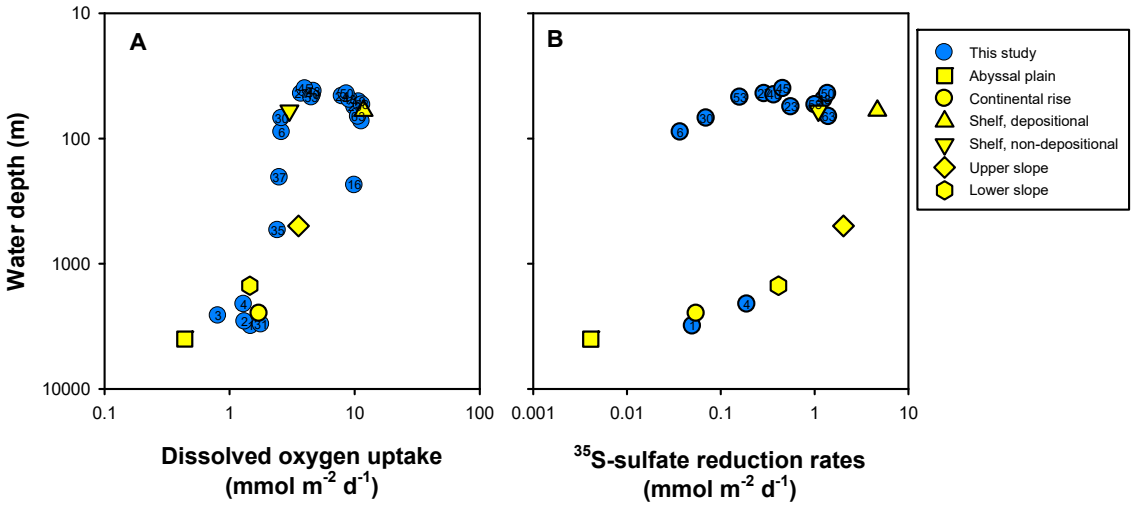

1110

1111 Fig. 9A. Water depth variation of sediment oxygen uptake. 9B: Water depth variation of integrated
1112 ^{35}S-sulfate reduction rates (0-30 cm sediment depth). For reference average rates of abyssal plain,
1113 continental rise, slope, and shelf sediments, deposition and non-depositional from Canfield et al.
1114 (2005).

1115